ELSEVIER

Journal of Magnetism and Magnetic Materials 200 (1999) 290–321

Journal of magnetism and magnetic materials

www.elsevier.com/locate/jmmm

Effect of roughness, frustration, and antiferromagnetic order on magnetic coupling of Fe/Cr multilayers

D.T. Pierce*, J. Unguris, R.J. Celotta, M.D. Stiles

Electron Physics Group, National Institute of Standards and Technology, Gaithersburg, MD 20899-8412, USA

Received 22 February 1999

Abstract

The interplay between interfacial disorder and the antiferromagnetic order in Cr leads to complex behavior in Fe/Cr multilayers. Measurements of interlayer coupling are discussed for samples with different amounts of disorder ranging from optimally fabricated trilayers of Fe/Cr/Fe on Fe(0 0 1) whiskers, to trilayers with increasing degrees of interfacial roughness, and finally to superlattices of Fe/Cr. The coupling of ferromagnets through noble-metal spacer layers can be described by a model that consists of bilinear coupling averaged over thickness fluctuations and extrinsic biquadratic coupling induced by the thickness fluctuations. This, the conventional model, also describes much of the behavior observed for Fe/Cr multilayers. However, in this case, the antiferromagnetism in Cr leads to results not explained by the conventional model. For nearly ideal interfaces, the Fe–Cr coupling can induce order in Cr, modifying the temperature dependence of the interlayer coupling. In addition, interfacial disorder can frustrate the antiferromagnetic order in the Cr, leading to a variety of ordered states which have been observed by neutron scattering. Each of these ordered states, in turn modifies the interlayer coupling in unexpected ways. The different ways in which the systems minimize the frustration can explain the experimental results.

Keywords: Magnetic multilayers; Interlayer exchange coupling; Interfacial disorder; Spin density wave

1. Introduction

Fe layers separated by Cr spacer layers have been at the center of many important discoveries related to magnetic coupling and transport properties. Fe/Cr/Fe trilayers exhibited the first evidence of antiferromagnetic coupling of two ferromagnetic layers through a transition-metal spacer layer [1]. Giant magnetoresistance was discovered in Fe/Cr multilayers [2,3]. Fe/Cr superlattices were among the first systems to show oscillations in the coupling between the layers as the Cr thickness was varied [4]. The existence of short-period as well as long-period oscillations was first seen in Fe/Cr/Fe trilayers [5,6]. In spite of the intense study of the Fe/Cr system as indicated by these many discoveries, there are still many unanswered questions and apparent discrepancies between experiments.

For noble-metal spacer layers, the interlayer exchange coupling is well described by quantum well models where the coupling properties are determined by the Fermi surface of the spacer-layer material and the reflection amplitudes for electrons scattering at the interfaces between the spacer layer

* Corresponding author. Fax: + 1-301-926-3746.
E-mail address: daniel.pierce@nist.gov (D.T. Pierce)

0304-8853/99/$ - see front matter
PII: S0304-8853(99)00319-4

and the ferromagnetic layers [7–10]. Good agreement has been obtained between quantum well model calculations and measured periods and strength of the oscillatory exchange coupling [11,12]. In contrast, measurements of Fe/Cr/Fe trilayers and Fe/Cr superlattices yield contradictory results on the following topics: observation of short-period versus long-period oscillatory coupling, coupled layers versus uncoupled Fe layers, collinear versus non-collinear coupling, commensurate versus incommensurate antiferromagnetic order in the Cr, etc. The disparate results are connected with the unique magnetic nature of Cr and the sensitivity of the Cr magnetic order and the interlayer exchange coupling to a variety of structural details.

The purpose of this paper is to review selected Fe/Cr multilayer coupling measurements, which may appear at first glance to be contradictory, and interpret them in a consistent framework. We attempt to take into account differences in sample structure and to synthesize various explanations into a coherent picture of the physics that shows how the disparate experimental results can be understood. Rather than attempting an encyclopedic review, we select experimental results to illustrate main points and point out areas of agreement and disagreement in light of current models. For this paper, we concentrate on the coupling of the Fe layers through Cr up to a thickness of about 10 nm, which is roughly the maximum distance over which exchange coupling is still observed.

Because interface structure is believed to be very important in determining the magnetic coupling, we will focus on three general classes of samples: (1) 'optimal trilayers', i.e., trilayer samples fabricated on Fe whiskers under conditions for optimum growth to approach, as closely as possible, ideal interfaces, (2) 'rougher trilayers', i.e., trilayers fabricated on Ag-buffered GaAs substrates and trilayers fabricated on Fe whiskers at lower temperatures, both of which have rougher Fe/Cr interfaces, and (3) 'superlattices', i.e., Fe/Cr superlattices with still rougher interfaces. After presenting the experimental facts for each of these classes, we discuss the theories and plausible explanations of the different behavior. Knowledge of the sample interfaces comes from sample characterization techniques like scanning tunneling microscopy (STM), reflection high-energy electron diffraction (RHEED) and X-ray diffraction (XRD). We discuss the magnetic coupling and Cr magnetic order in the samples measured with a variety of techniques: scanning electron microscopy with polarization analysis (SEMPA), magneto-optic Kerr effect (MOKE), Brillouin light scattering (BLS), neutron scattering, and perturbed angular correlation spectroscopy (PACS).

The organization of the paper is as follows. The next three sections give background information on the special characteristics of Cr as a spacer layer (Section 2), the important length scales and origin of spin frustration (Section 3), and the conventional model for describing interlayer exchange coupling (Section 4). The next six sections come in pairs presenting first the experimental results and then the interpretation for each of the three classes of samples: optimal trilayers (Sections 5 and 6), trilayers with varying interfacial roughness (Sections 7 and 8), and superlattices (Sections 9 and 10). Conclusions are presented in Section 11. We list some symbols used frequently in this paper in Table 1.

Table 1
Commonly used symbols. List of symbols that are commonly used in the paper. Unaveraged coupling strengths are defined for discrete thicknesses *nd*, and averaged coupling strengths are defined for continuous average thickness *t*

Symbol	Definition
d	Cr layer spacing
n	Number of layers
σ	rms roughness
σ_{Fe}	Roughness at lower trilayer interface
σ_{Cr}	Roughness at upper trilayer interface
σ_t	Standard deviation of Cr thickness distribution
R	Mean island spacing
L	Terrace length
l	Lateral response length of Fe
$J_1(n)$	Unaveraged bilinear coupling
$\bar{J}_1(t)$, $\bar{J}_1$	Averaged bilinear coupling
$\bar{J}_2(t)$, $\bar{J}_2$	Averaged biquadratic coupling
$J_S(n)$, J_S	Unaveraged short-period coupling
$\bar{J}_S$	Averaged short-period coupling
ΔJ_S	Difference in $J_S(n)$ for thicknesses differing by one layer

2. Special characteristics of Cr as a spacer layer

In its paramagnetic state, Cr has considerable portions of its Fermi surface nearly parallel, or nested, as seen in Fig. 1 and labeled with the wave vector $\boldsymbol{Q}$. The unenhanced susceptibility $\chi_0(\boldsymbol{q})$ is therefore peaked at $\boldsymbol{q} = \boldsymbol{Q}$. When electron–electron interactions are included we get the enhanced susceptibility

$$\chi(\boldsymbol{q}) = \chi_0(\boldsymbol{q})/[1 - I\chi_0(\boldsymbol{q})], \quad (1)$$

where I, the enhancement factor, accounts for exchange and correlation [13]. The large susceptibility at $\boldsymbol{Q}$ leads to a transition from paramagnetic Cr to antiferromagnetic order as the temperature decreases below the Néel temperature T_N. The nesting wave vector $\boldsymbol{Q}$ is slightly incommensurate with the lattice wave vector π/d, i.e., $Q = \pi(1 - \delta)/d$ where δ is the incommensurability parameter [13]. The layer spacing is d which equals $a/2 = 0.144$ nm, where a is the lattice constant. When Cr orders antiferromagnetically, a small gap opens at the Fermi level and that part of the nested Fermi surface connected by $\boldsymbol{Q}$ in Fig. 1 disappears. This behavior is associated with resistivity anomalies in bulk Cr [13,14].

The antiferromagnetic order of Cr has complex variations. Commensurate antiferromagnetic order is the simplest, as illustrated in Fig. 2a. The magnetic moments of the Cr atoms are all of the same magnitude and alternate in direction with each Cr layer in a [0 0 1] direction. This type of AF order is seen in Cr alloyed with, for example, small amounts of Mn [13,14]. In pure bulk Cr, the antiferromagnetic order leads to an incommensurate spin density wave (ISDW) with a periodic modulation of the Cr magnetic moment,

$$\mu = \mu_0 \cos(Q'z) = \mu_0(-1)^n \cos(n\delta'\pi), \quad (2)$$

where $\mu_0 = 0.62\ \mu_B$ for bulk Cr at zero temperature, and the SDW ordering wave vector is $Q' = \pi(1 - \delta')/d$. The SDW ordering wave vectors are always closer to commensuration than the nesting wave vectors $\boldsymbol{Q}$, i.e., $0 < \delta' < \delta$ [15]. The distance between nodes is d/δ'. The Cr moments can be perpendicular to $\boldsymbol{Q}$ to form a transverse SDW as illustrated in Fig. 2b. The moments can also be parallel to $\boldsymbol{Q}$ forming a longitudinal SDW that is observed in bulk Cr at temperatures below 123 K. Commensurate, transverse ISDW and longitudinal ISDW are also referred to as AF0, AF1, and AF2 order, respectively.

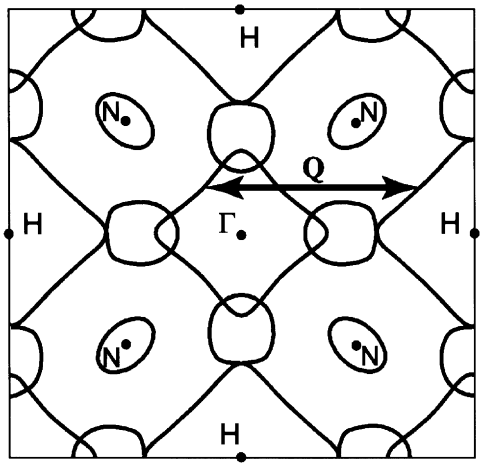

Fig. 1. A slice through the paramagnetic Cr Fermi surface for an interface in the (0 0 1) direction. The wave vector $\boldsymbol{Q}$ connects parallel 'nested' regions of the Fermi surface.

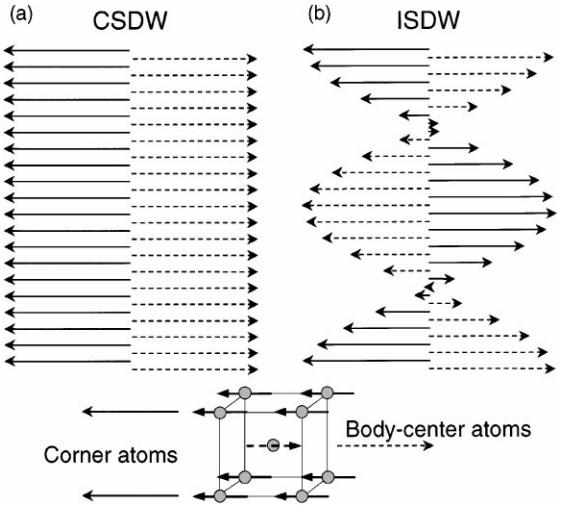

Fig. 2. (a) Commensurate antiferromagnetic order is shown where the solid arrows and dashed arrows represent the Cr moments on corner atom and body-center atom sites, respectively. (b) One period of an incommensurate spin density wave (ISDW) is illustrated showing the variation of the Cr moments.

3. Length scales and spin frustration

We first consider how to describe the roughness at an interface. A measure of the lateral distribution of the roughness can be obtained by calculating the height–height correlation function, for example from STM images. The height–height correlation is defined as $G(r) = \langle \Delta h(r + r')\Delta h(r') \rangle$ where $\Delta h(r') = h(r') - \langle h(r') \rangle$ is the deviation of the local height, measured here in monolayers (ML), from the average height, and $\langle \text{- - -} \rangle$ denotes the spatial average over all points r' within the region of interest. The rms roughness at the interface is $\sigma = (G(0))^{1/2}$. The first peak in $G(r)$ gives the mean separation between typical features, R, which for simplicity we will refer to as the mean island separation. An important length for the discussion of the coupling is the average terrace length L. For a given R, the average terrace length L, in a simple model, decreases with increasing σ, that is $L \propto R/\sigma$.

We distinguish between interface roughness and thickness fluctuations. If there is a step at the bottom interface of the Cr spacer layer that is replicated at the upper interface, the roughness due to this step is fully correlated and there is no thickness fluctuation. If the lower interface is flat over the region of interest, as may be the case with an Fe whisker, the thickness fluctuations are completely specified by the σ of the upper interface. For arbitrary interfaces, the standard deviation of the thickness distribution, σ_t, depends on the roughness of both interfaces which can be correlated to varying degrees. For simplicity, consider a trilayer with roughness at the lower interface, σ_{Fe}, and at the upper interface, σ_{Cr}. Then, in general, $\sigma_t^2 = \sigma_{Fe}^2 + \sigma_{Cr}^2 - 2\langle \Delta h_{Fe} \Delta h_{Cr} \rangle$, where we have suppressed the spatial arguments that are averaged over. We consider two limiting cases: (1) the roughness at the upper interface and the roughness at the lower interface are not correlated, $\langle \Delta h_{Fe} \Delta h_{Cr} \rangle = 0$, so that $\sigma_t^2 = \sigma_{Fe}^2 + \sigma_{Cr}^2$, or (2) the Cr thickness fluctuations and the roughness at the lower interface are not correlated, $\langle \Delta h_{Fe} \Delta t \rangle = 0$, so that $\langle \Delta h_{Fe} \Delta h_{Cr} \rangle = \langle \Delta h_{Fe}(\Delta h_{Fe} + \Delta t) \rangle = \sigma_{Fe}^2$ and $\sigma_t^2 = \sigma_{Cr}^2 - \sigma_{Fe}^2$. Thus, for these two simple cases, the standard deviation of the thickness fluctuations is either $\sigma_t = (\sigma_{Cr}^2 + \sigma_{Fe}^2)^{1/2}$ or $\sigma_t = (\sigma_{Cr}^2 - \sigma_{Fe}^2)^{1/2}$. Depending on the growth-induced correlation between the interfaces, the standard deviation of the thickness fluctuations can be greater or lesser than the rms roughness of the upper interface.

The spin configuration in the Fe and Cr layers is affected by interface roughness. In a local moment model, the Fe–Fe interactions favor ferromagnetic alignment of spins, while the Cr–Cr and Cr–Fe interactions favor antiferromagnetic alignment. For perfect interfaces, there are spin configurations, as in Fig. 3a, in which all pairs of spins have their preferred alignment. If there is roughness at the interface as shown in Fig. 3b–Fig. 3d, it is not possible to obtain the preferred alignment for all pairs of spins. Some pairs will necessarily not be in their minimum energy configuration, that is, the coupling will be 'frustrated'. For the same structure there can be many plausible spin configurations that are local minima of the energy [16–18]. In Fig. 3b, the Fe–Fe and Fe–Cr interactions are satisfied, but the Cr–Cr interactions are frustrated through the Cr film at the position of the steps in the interface. The frustration of the Fe–Cr interaction at the interface is shown in Fig. 3c and in Fig. 3d the frustration is taken up in the Fe layer.

The energy minimization that determines where the frustration occurs will depend on the relative sizes of several length scales such as the thickness of the Fe and Cr layers and the vertical and lateral extent of the interfacial defects. It will also depend on the strength of the interactions and on the temperature since the interactions are temperature

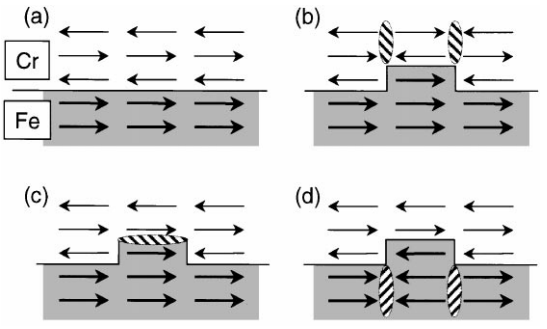

Fig. 3. Relieving spin frustration at an Fe/Cr interface. (a) Perfect interface, no frustration. (b) Frustration caused by a step is relieved by a wall in the Cr. (c) Frustration relieved at the interface. (d) Frustration relieved by walls in the Fe.

dependent. It is expected that the Cr–Cr interaction will be more temperature sensitive since the bulk Cr Néel temperature, $T_N = 311$ K, is much smaller than the Fe Curie temperature, $T_C = 1043$ K. Precise values are not available for the strengths of the Fe–Fe coupling, the Fe–Cr coupling, and the Cr–Cr coupling. Typical estimates of the relative strengths of the Fe–Fe, Fe–Cr, and Cr–Cr coupling are 1: −0.3: −0.18 [15][1] and 1: −0.55: −0.3 [19]. Roughly speaking, these estimates have the Fe–Fe coupling about two to three times the antiferromagnetic Fe–Cr coupling which in turn is about two times the Cr–Cr coupling. This suggests that it costs less energy for the interface frustration region of Fig. 3c to be in the Cr rather than right at the interface [16]. The lines drawn in Fig. 3 to represent the frustration are only schematic. Generally, not much is known about these regions; for example, we do not know whether the change is fairly abrupt or spread out over many lattice constants.

Local moments coupled to each other, as shown schematically in Fig. 3, can be a good description of Cr with commensurate antiferromagnetic order. However, it should be remembered, that Cr is an itinerant antiferromagnet. This distinction is particularly important when Cr is in an incommensurate order state. The intineracy may lead to more variation in the moments than is expected from local moment models. This variability of the size of the moments complicates even further the determination of the minimum energy state for a frustrated system.

There are also magnetic length scales that must be considered. Of particular importance is the length over which the magnetization in Fe can reverse its direction, which we call the lateral response length l. This length can be estimated, in the simplest approximation, as the domain wall width in bulk Fe. The Bloch wall width in bulk Fe is given by $l = \pi(A_{ex}/K)^{1/2} \approx 66$ nm, where the exchange constant, $A_{ex} = 2.1 \times 10^{-11}$ J/m, and the cubic crystal anisotropy constant, $K = 4.7 \times 10^4$ J/m^3. The exchange energy tends to increase the wall width to achieve a slow spatial variation of spin direction. The anisotropy, on the other hand, tends to decrease the wall width to reduce the number of spins pointing in hard directions. In the Fe/Cr multilayer, the interlayer coupling behaves like an anisotropy that favors the Fe magnetization in a given direction. When the interlayer coupling dominates other anisotropies, one can write [20] $l = \frac{1}{2}\pi(A_{ex}t_{Fe}/J_1(n))^{1/2}$ where t_{Fe} is the thickness of the Fe layer and $J_1(n)$ is the interlayer coupling strength at the discrete Cr layer thickness nd [20]. For a thin Fe film in the Fe/Cr/Fe trilayer, the magnetization will turn in a plane parallel to the interface as a Néel wall. In a more detailed calculation of the wall width, the anisotropy, the interlayer coupling, and any other contributions to the energy must be included. Rührig and Hubert calculated an Fe wall width of 150 nm for 30 nm thick Fe layers separated by 13 ML of Cr; this value agreed well with their measurements [21].

Less is known about magnetic transition lengths in Cr. Some calculations find that the frustration can reduce the moments, reducing in turn the length scale required to relieve frustration [16,17,22]. In other cases frustration may lead to rotation of the moments [23–25]. Determinations of the minimum energy magnetic order in the presence of frustration will depend strongly on the model used to describe the Cr. While the model calculations of defect structures done to date give an indication of what might happen, they are not definitive because they do not include all the important physics. In particular, these model calculations do not describe antiferromagnetism in Cr sufficiently accurately to produce incommensurate order in bulk Cr.

4. The conventional model

We present briefly the model most commonly used in describing the exchange coupling of magnetic layers in order to provide a structure for our later discussion of numerous experimental results. In the conventional model the coupling is described

[1] The Cr–Cr estimate is the mean field result for a Heisenberg antiferromagnet. On the other hand, an estimate of the Cr–Cr coupling from the spin wave velocity is eight times larger. These values emphasize the difficulty of estimating the Cr–Cr coupling in an itinerant spin wave system. (R.S. Fishman, private communication.)

by a bilinear coupling term and a biquadratic term. The model assumes a paramagnetic spacer layer in an itinerant electron picture. Thickness fluctuations of the spacer layer average the coupling, so short-period couplings are not observed if the thickness fluctuations are too large. The thickness fluctuations also lead to the biquadratic coupling. Beginning in Section 6, we will discuss departures from this conventional model owing to the special nature of Cr.

The total coupling energy per unit area, E_c, is described in a phenomenological model that was proposed to explain certain experimental observations [26,27].

$$E_c = -\bar{J}_1 \hat{\boldsymbol{m}}_1 \cdot \hat{\boldsymbol{m}}_2 - \bar{J}_2 (\hat{\boldsymbol{m}}_1 \cdot \hat{\boldsymbol{m}}_2)^2 = -\bar{J}_1 \cos(\theta) - \bar{J}_2 \cos^2(\theta). \quad (3)$$

The first term in this equation is the Heisenberg-like exchange term. The bar is used to emphasize that the measured quantities are averaged values. Depending on the sign of $\bar{J}_1$, the magnetization directions of the two Fe layers, given by unit vectors $\hat{\boldsymbol{m}}_1$ and $\hat{\boldsymbol{m}}_2$, will be parallel or antiparallel. The coupling depends on $\hat{\boldsymbol{m}}_1 \cdot \hat{\boldsymbol{m}}_2$, i.e., it is bilinear in the magnetization directions. The second term, called the biquadratic coupling term since it is biquadratic in $\hat{\boldsymbol{m}}_1$ and $\hat{\boldsymbol{m}}_2$, leads to canted or non-collinear coupling, that is different from 0° or 180°, when $\bar{J}_2 < 0$ and $|\bar{J}_1| < -2\bar{J}_2$. Minimizing E_c with respect to θ gives the angle of the canted coupling as $\cos\theta = -\bar{J}_1/2\bar{J}_2$. To find the minimum energy state of a multilayer, in the general case, it is necessary to include not just the terms in Eq. (3) but also other terms such as the anisotropy energies of the magnetic films [26,28,29].

In the conventional model, the materials are treated in an intinerant electron picture. For a paramagnetic spacer layer, the interlayer coupling is determined by the spin-dependent reflections at the interfaces between the spacer layer and the ferromagnet layers [7–10]. The periods of the oscillatory coupling are determined from the critical spanning vectors of the spacer-layer Fermi surface. The strength of the coupling depends on the Fermi surface geometry and the reflection amplitudes of electrons at the interfaces between the spacer layer and the ferromagnetic layers. For paramagnetic Cr, assuming two contributions to the oscillatory coupling, as observed, J_1 can be written

$$J_1(n) = J_S(n) + J_L(n) = (1/nd)A_S \sin(2\pi nd/\Lambda_S + \Phi_S) + (1/n^2d^2)A_L \sin(2\pi nd/\Lambda_L + \Phi_L), \quad (4)$$

where Λ_S and Λ_L are the short and long periods, respectively, Φ_S and Φ_L are the phases, and the amplitudes A_S and A_L include all the Fermi surface geometry and interface reflection probabilities. The $1/nd$ thickness dependence for the short-period oscillation is unique to Cr because there is full planar nesting. Not shown in Eq. (4) are additional factors arising from effects of temperature and disorder that further decrease the coupling with increasing spacer layer thickness [30]. This model only applies to paramagnetic Cr. When the Cr is antiferromagnetic, a gap opens at the Fermi level [13] and quantum well models can no longer be used to describe the two-layer short-period coupling. In this case, the antiferromagnetic order determines the short-period coupling.

The short- and the long-period parts of the coupling, $J_S(n)$ and $J_L(n)$, are defined only at each discrete thickness nd. In realistic spacer layers, there are thickness fluctuations which act, within a region defined by the lateral response length l of the magnetic layer, to average the coupling contributions from regions of different thickness. Thus, one measures an average coupling,

$$\bar{J}_1(t) = \bar{J}_S + \bar{J}_L = \sum_n P(t, n)\, J_S(n) + \sum_n P(t, n)\, J_L(n), \quad (5)$$

where $P(t, n)$ is the fraction of the interlayer area that is n layers thick when the average thickness is t. Thus, short-period oscillatory coupling will be more rapidly averaged out by the thickness fluctuations than the long-period coupling.

When the average bilinear coupling $\bar{J}_1$ becomes small enough, as a result of spacer-layer thickness fluctuations, the multilayer finds its minimum energy state when the magnetic moments of the Fe layers turn into a direction perpendicular to each other. This is the basis of the model proposed by Slonczewski [31] that takes into account the

fluctuations $\Delta J_1(n)$ in the bilinear coupling as the coupling $J_1(n)$ changes sign from one discrete layer thickness to the next. In the case of Cr, the unaveraged $J_S(n)$ is larger than unaveraged $J_L(n)$ and dominates the contribution to the biquadratic coupling so $\Delta J_1(n) \cong \Delta J_S(n)$. When the overlayer thickness t_{Fe} is small compared to the characteristic length scale L of the terraces producing the thickness fluctuations, the leading contribution to the biquadratic term in this model is

$$\bar{J}_2 \propto -(\Delta J_1)^2 L^2 / A_{ex} t_{Fe} = -(\Delta J_S(n))^2 L^2 / A_{ex} t_{Fe}, \tag{6}$$

where A_{ex} is the intralayer exchange coupling which hinders magnetization reversals, as would be dictated by fluctuations in the bilinear coupling, over the lateral response length l. The model is invalid when $L > l$.

Other models have been proposed to explain biquadratic coupling. Intrinsic theories that consider ideal systems with perfect interfaces predict biquadratic contributions that are much smaller than what is observed [32]. The dipole fields resulting from rough interfaces in the layered system provide another extrinsic mechanism that is always present to some degree. Biquadratic coupling from this mechanism is independent of the material parameters for non-magnetic spacer layers. An estimate of its size for 0.5–1 nm roughness with a characteristic length scale of 20–50 nm gives $\bar{J}_2 = 0.01\ \mathrm{mJ/m^2}$. This contribution decreases for smaller L and larger spacer-layer thickness [32,33]. While it must always be considered, it is likely smaller than other contributions in the samples considered here.

As an alternative to the conventional model, Eqs. (3)–(6), we mention the *torsion* or *proximity* model that depends on the intrinsic antiferromagnetic stiffness of a spacer layer like Cr or Mn and is sometimes invoked to explain the resulting special behavior [23]. A strong Fe–Cr interaction is assumed such that the proximity of the Fe leads to a commensurate antiferromagnetic structure in the Cr that persists even above its bulk T_N. For an odd or even number of Cr layers, the minimum energy state has the Fe layers coupled with magnetization directions parallel or antiparallel, respectively. If there are thickness fluctuations so that both odd and even Cr thicknesses are present, the energy is minimized by the Cr moments in the region with an odd number of layers winding like a torsion spring with one sense, and regions with an even number of layers with the opposite sense, to reach the same average direction of the top Fe layer [23]. The coupling per unit area is given by

$$E_c = J_{odd}\theta^2 + J_{even}(|\theta| - \pi)^2, \tag{7}$$

where $-\pi < \theta < \pi$ and J_{odd} and J_{even} are the coupling functions associated with areas where the number n of Cr layers is odd and even, respectively [23–25]. For n odd, Eq. (7) is minimized for $\theta = 0$ and the Fe layers are ferromagnetically coupled. For equal regions of odd and even layers, $\theta = \pi/2$. The general case of Cr thickness fluctuations in this model leads to non-collinear coupling. Another consequence of this model is that for any small thickness fluctuations there are both odd and even thicknesses present. In this case, the magnetization remains at a finite (not 0 or π) angle for all applied fields, giving hysteresis curves with a gradual approach to saturation.

We have just described two models for the interlayer coupling, the conventional model and the torsion model, based on the simplest possible approximations for the variation of the energy as a function of the relative orientation of the moments of the two magnetic layers, given by the angle θ. In the conventional model we assume that for ideal interfaces, the energy as a function of this angle of the moments varies as $-J_1 \cos(\theta)$, with the sign of J_1 depending on whether parallel or antiparallel alignment is preferred. In the torsion model, the coupling energy is assumed to vary as $J(\theta)^2$ or $J(|\theta| - \pi)^2$ depending on whether parallel or antiparallel alignment is favored. The correct model will have to describe both the itineracy of the electrons as represented by the conventional model and the atomic-like correlations as represented by the local moments in the torsion model. Calculations of the variation of the energy as a function of relative magnetization angle using tight-binding [24,25] for six layers of Cr gave a result consistent with the form assumed in the torsion model. For less than six Cr layers, these calculations gave significant deviations from that form. While

calculations have not been carried out for thicker films, the functional form is also likely to be more complicated than either of the simple limits described above, particularly when the incommensurate state of Cr becomes energetically competitive with the commensurate state. Since there are no calculations for thick Cr spacer layers that allow twisting of moments and the formation of the incommensurate state, the correct angular variation of the energy is not known. In this paper, we will analyze the results using the form $-J_1\cos(\theta)$. We will show that there are very few results that are inconsistent with this form, which only shows that it can be difficult to differentiate between these forms. Whatever the form of the angular variation, it is necessary to consider the different possible ways to relieve the frustration that will be present with disorder, as discussed in Section 3.

5. Optimal trilayer structures: measurements

5.1. Sample preparation

The starting point for nearly ideal Fe/Cr/Fe trilayer structures is an Fe single-crystal whisker. Fe whiskers are typically a few tenths of a mm wide and 10–20 mm long with $\langle 1\,0\,0\rangle$ faces. The whiskers are cleaned by ion bombardment and annealing [34]. Whisker surfaces can have approximately 1 μm terraces between single atom steps [35]. This corresponds to a misalignment from a perfect (0 0 1) surface of less than 0.01°. There is some variation in step density between whiskers and over a given whisker; terraces a few hundred nm wide have also been observed. For growth of the Cr film nearest to the layer-by-layer ideal, RHEED studies of intensity oscillations and diffraction spot width have shown that the optimum temperature range of the Fe whisker substrate is $550 < T_{s,opt} < 590$ K [36]. Fig. 4 shows an STM image of a 3.7 ML thick Cr film grown at $T_s = 573 \pm 20$ K [37].[2] The layer-by-layer character of the Cr growth is clearly evident. The mean island separation, R, in Fig. 4, is

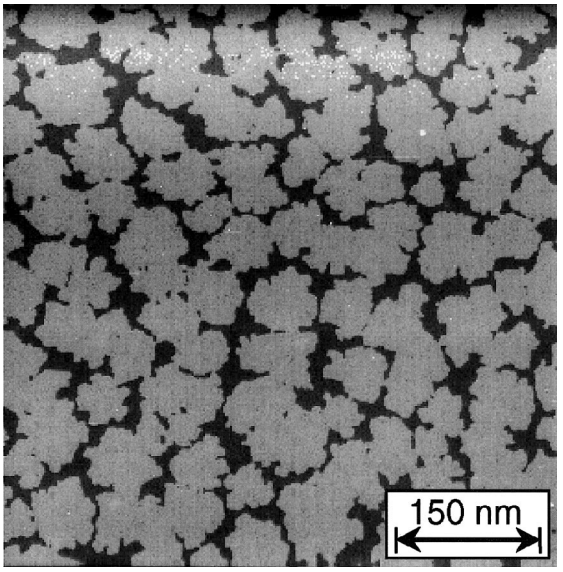

Fig. 4. An STM image of 3.7 ML of Cr evaporated on an Fe whisker at 573 K. The large single atom high islands show layer-by-layer growth [37].

determined from a height–height correlation analysis to be 85 ± 10 nm.

However, at the optimum temperature for layer-by-layer growth, there is some interchange of the deposited Cr atoms and the Fe substrate atoms at the interface leading to an interfacial alloy. This can be seen in the STM image of 0.4 ML Cr deposited on the Fe shown in Fig. 5a [38,39]. A single atom high island is evident, as are many little bumps both on the substrate and the island. Unique surface states on Fe(0 0 1) and Cr(0 0 1) allow positive identification by scanning tunneling spectroscopy of the bumps as spectroscopic features derived from Cr atoms [40]. Thus, the islands contain Fe as well as Cr and there are Cr atoms in the Fe substrate. Angle-resolved Auger studies of 0.5 ML Cr deposited at 570 K on Fe(0 0 1) found that about half of the Cr deposited goes into the first two layers of the substrate and about half remains in the first adlayer as shown in Fig. 5b [36,41,42]. The alloying can be reduced by growing the first layer or first few layers of Cr at a reduced temperature followed by increasing the temperature to $T_{s,opt}$ [36]. Proton-induced Auger spectroscopy has also shown evidence of alloying at the interface [43]. Scanning tunneling

[2] Uncertainties reported in this paper represent one standard deviation and include both statistical and systematic errors.

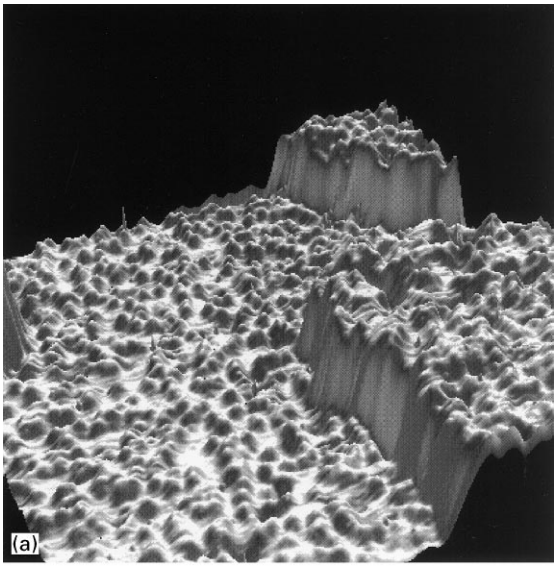

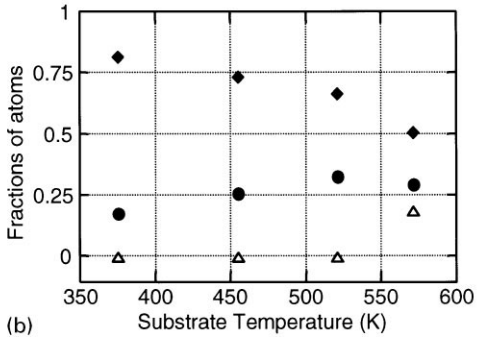

Fig. 5. (a) A rendered perspective STM image of 0.4 ML deposited on Fe at 563 ± 10 K. The small bumps on the Fe whisker substrate and on the one-atom high islands (much expanded vertical scale) are Cr atoms which have interchanged with Fe atoms to create an interfacial alloy [38]. (b) The results of angle-resolved Auger measurements of the substrate temperature dependence of the fraction of deposited Cr atoms in the adlayer (◆), in the first (surface) Fe layer of the whisker (•) and in the second (subsurface) Fe layer (△) [36].

spectroscopy measurements indicate that the second layer deposited is predominantly Cr [38,39]. When Heinrich et al. intentionally deposited a mixed layer of Fe and Cr at the interface, they found that it behaved as if the Fe–Cr alloy was part of the Fe film for Fe concentrations >15% [36]. The consequences of interfacial alloying for the coupling are discussed below. It has been suggested that the Fe overlayer is not as susceptible to

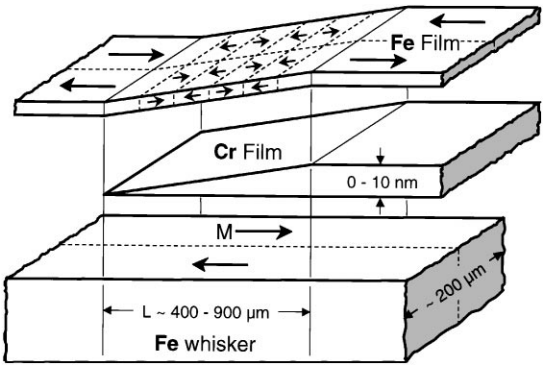

Fig. 6. A schematic exploded view of the wedge trilayer sample structure showing the Fe(0 0 1) single-crystal whisker substrate, the evaporated Cr wedge, and the Fe overlayer. The arrows in the Fe show the direction of magnetization in each domain. The vertical scale is expanded many times.

alloying with the Cr spacer layer [36]. In any case, the growth of an Fe overlayer at room temperature is adequate for completing a good trilayer.

Results from two types of optimal trilayers are presented. The MOKE and BLS measurements [36] discussed in this section were made on Fe/Cr/Fe(0 0 1) trilayers with Cr layers of uniform thickness using RHEED to monitor the completion of each full layer. The SEMPA measurements, on the other hand, were carried out on a trilayer structure where the average Cr spacer thickness increases linearly over a distance of approximately 1 mm as shown in Fig. 6 [5]. This wedge-shaped Cr spacer provides a sample that contains a linearly varying range of thicknesses, all prepared under the same growth conditions. The slope of the Cr wedge is typically such that the Cr thickness increases 1 ML over 10 μm. No changes in the magnetic properties were observed for wedges twice as steep or ten times less steep [44].

5.2. SEMPA observations of short-period oscillations in the magnetic coupling

Short-period oscillations in the magnetic coupling are strikingly displayed by the SEMPA image of the magnetization, along the length of the whisker, shown in Fig. 7a [45]. The SEMPA image is formed by measuring the spin polarization of the secondary electrons as the SEM beam is rastered

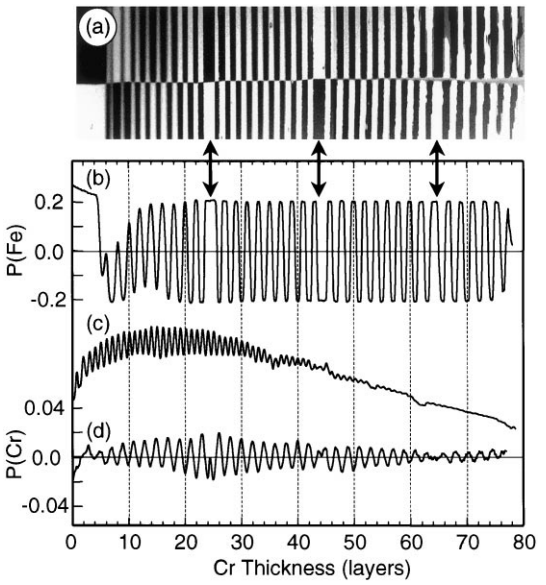

Fig. 7. (a) SEMPA image of the component of magnetization, M_x, in the Fe overlayer along the Fe whisker. The arrows mark the Cr spacer-layer thicknesses where phase slips in the short-period oscillations of the magnetization occur. (b) A line scan through (a) showing the measured spin-polarization profile of the overlayer. (c) Spatial RHEED intensity oscillations along the Cr wedge before depositing the Fe overlayer give an accurate determination of Cr thickness. (d) The spin polarization of the Cr layer P(Cr), before depositing the Fe overlayer, after subtracting the background from the whisker.

across the sample surface. SEMPA is a surface-sensitive technique that gives a polarization image proportional to the magnetization in the top few layers of the specimen [46,47]. The opposite contrast in the top and bottom half of the magnetization image of the Fe overlayer in Fig. 7a results from the coupling through the Cr spacer layer to the Fe whisker which has two domains with magnetization in opposite directions as illustrated in Fig. 6. The Fe overlayer is seen to be coupled ferromagnetically to the Fe whisker substrate for the first four layers, and then the coupling begins to oscillate, changing from ferromagnetic to antiferromagnetic (overlayer magnetization antiparallel to the whisker magnetization) and back as the Cr increases by two additional layers. This can be seen clearly in Fig. 7b, which shows the profile of the polarization from Fig. 7a. This change in the direction of the coupling continues with each additional Cr layer up to 24 layers. The 24th and 25th layers are both coupled ferromagnetically and only at the 26th layer does the coupling switch to antiferromagnetic. At room temperature, where this was measured, this phase slip in the coupling is repeated each subsequent 20 layers as noted by the arrows in Fig. 7.

Before the Fe overlayer was deposited for the measurements displayed in Fig. 7a and Fig. 7b, the thickness and magnetization of the bare Cr were measured. It is possible to scan the SEM beam along the wedge at grazing incidence and observe RHEED intensity oscillations as it moves from a thickness where the top Cr layer is partially filled, to a position where it is filled, and so on [5]. The RHEED intensity oscillations measured in this way are shown in Fig. 7c. The decrease in intensity with increasing thickness correlates with the expected increase in roughness. The RHEED oscillations not only help characterize the quality of film growth, but act as a very accurate ruler to give the thickness at each position of the wedge to ± 0.1 layer. This, along with the observation of the short-period oscillations in the coupling over many periods, allowed us to accurately determine the short period, $\Lambda_S = 2.105 \pm 0.005d$ [48].

The SEMPA measurement of the bare Cr polarization P(Cr) is shown in Fig. 7d after subtracting an exponential to reduce the background from the Fe whisker that is significant for about the first 10 ML of Cr. Note that the magnitude of P(Cr) is much smaller than the polarization measured for the Fe overlayer P(Fe). The $1/e$ sampling depth in Cr for the electrons measured by SEMPA is $3.8 \pm 0.3d$ [45] so even though the top Cr layer dominates P(Cr), subsurface moments with alternating directions reduce the measured value. Comparing P(Cr) and P(Fe) in Fig. 7b and Fig. 7d, it can be seen that the polarization of the Fe overlayer is opposite to that of the Cr at Cr thicknesses of 5 ML and above. This is consistent with antiparallel coupling at the top Fe–Cr interface assuming that the Cr polarization direction does not change on the addition of an Fe overlayer. Antiparallel Fe–Cr coupling was also found in spin-polarized photoemission measurements [49,50].

Like P(Fe), we see that P(Cr) changes sign with each single layer increase in Cr thickness except for

the phase slips at 24–25, 44–45, and 64–65 layers. Up to the first phase slip, for antiferromagnetic Fe–Cr coupling at both interfaces and antiferromagnetic stacking of the Cr, we expect the Fe layers of the trilayer to be coupled ferromagnetically for an odd number of Cr layers and antiferromagnetically for an even number of Cr layers. Just the opposite is observed in Fig. 7b. This one layer offset has been attributed to the alloyed region approximately one layer wide at the interface observed for this high-temperature growth of Cr on Fe [36,38,39,41,42,51].

5.3. Temperature dependence of the phase slips

The SEMPA measurements described thus far were made at room temperature, that is, in the neighborhood of the Cr bulk Néel temperature, $T_N = 311$ K. It was found that as the sample temperature during the SEMPA measurement of a bare Cr wedge on the Fe(0 0 1) whisker was varied between room temperature and $1.8T_N$, the Cr thickness at which phase slips occurred varied reversibly [45]. The amplitude of the oscillations of P(Cr) changed less than 20% on heating to $1.8T_N$. The displacement by 14 layers of the position of the first phase slip from its position at 24–25 at 310 K to 38–39 layers at 550 K is displayed in Fig. 8a. The phase of the oscillations below 24 layers was not observed to change in this temperature range. Also shown in Fig. 8a is the distance between phase slips in bulk Cr measured by neutron scattering [52].

The change in the thickness where the first phase slip occurs can also be seen in the SEMPA measurements of an Fe/Cr/Fe trilayer at a series of measurement temperatures shown in Fig. 8b [53]. It is somewhat more difficult to locate the phase slips as a function of temperature in the trilayer data compared to bare Cr on Fe data because the short-period coupling strength drops off more rapidly with temperature than the long period. Only short-period oscillations are seen in the polarization P(Cr) of the bare Cr. The heavy line marking the change in the position of the phase slip in the trilayer with temperature is taken from the P(Cr) data of Fig. 8a. Where short-period oscillations can be seen above and below the phase slip line, for example at a Cr thickness of 30 layers, the magnetization direction is reversed. The dashed line is the same curve displaced 20 layers. There is some evidence of the magnetization reversal at 46–48 layers, e.g., compare the room-temperature data with that above the dashed line at approximately 425 K. All of these measurements are completely reversible and are not due to an irreversible roughening of the trilayer structure.

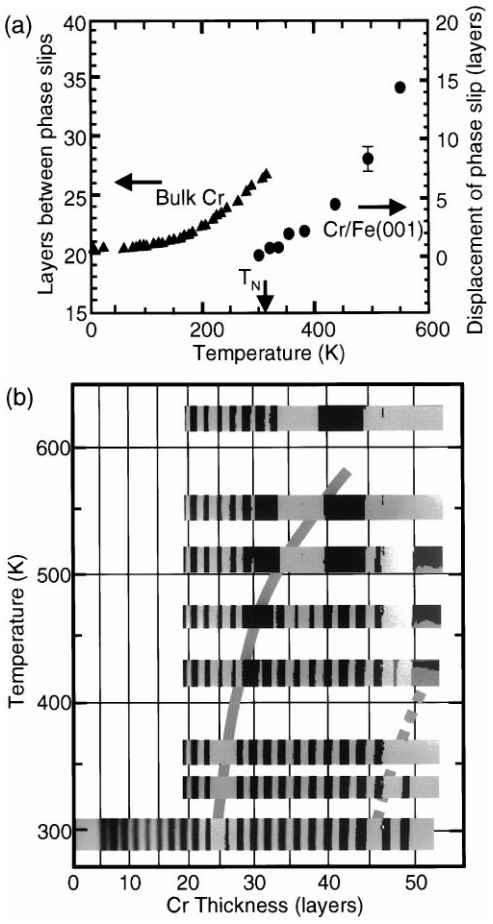

Fig. 8. (a) The temperature dependence of the number of layers between phase slips for bulk Cr [52] and the change in position of the phase slip in Cr/Fe(0 0 1) with temperature. The Néel temperature for bulk Cr is marked by the arrow. (b) Temperature dependence of SEMPA images indicating the bilinear coupling in Fe/Cr/Fe(0 0 1). The phase slips measured on the bare Cr are shown by the solid gray line; the dashed line is the estimated position of the next phase slip. Note that, where visible, the short-period oscillations have opposite direction above and below these lines.

5.4. Observation of non-collinear coupling of the Fe layers

The SEMPA image of Fig. 7a shows the Fe overlayer magnetization component along the whisker parallel to the magnetization of the whisker substrate, defined here as M_x. A similar image from a different trilayer wedge sample is shown in Fig. 9a [5]. The varying width of the black and white contrast in Fig. 9a is evidence of the long (12 ML) period coupling superimposed on the short-period coupling. Simultaneously measured with such an image are the intensity image, which gives topography information, and the image of the orthogonal in-plane component of the magnetization, M_y. The magnetization $\boldsymbol{M}$ lies in the plane of the Fe film and has constant magnitude, $|\boldsymbol{M}| = (M_x^2 + M_y^2)^{1/2}$. The direction of $\boldsymbol{M}$ is given by the angle, $\theta = \tan^{-1}(M_y/M_x)$. Fig. 9b and Fig. 9c show enlarged angle maps of the magnetization direction from the Cr thickness regions outlined in Fig. 9a. In the thinner part of the wedge, Fig. 9b shows that the Fe overlayer does not alternate between parallel and antiparallel, but instead between canted and roughly antiparallel. This canted coupling observed in the thin part of the Cr wedges varies from sample to sample due to slight differences in preparation. A variation in the coupling angle across the whisker is visible in Fig. 9b and highlighted by the line scans of Fig. 9d. In the thicker part of the wedge, Fig. 9c shows that where M_x becomes small as it goes through zero and reverses direction, there are regions of orthogonal magnetization, M_y shown in red and blue, i.e., there is 90° coupling. Of interest for later discussion, is the fact that the 90° coupling regions become narrower at a Cr thickness near 24 ML where the phase slip occurs.

The first observation [26] of such regions of 90° coupling was in Kerr microscopy studies of Fe/Cr_{wedge}/Fe trilayers grown on Ag-buffered GaAs substrates. These structures exhibited long-period coupling. In the transition region between the ferromagnetically and antiferromagnetically coupled regions, the coupling of the two Fe layers was at 90°. These experiments led to the addition of the biquadratic coupling term to obtain Eq. (3) [26]. A similar equation was proposed to explain the hysteresis loops observed in Co/Cu structures [27].

5.5. Strength of the interlayer exchange coupling

The strength of the interlayer exchange coupling, i.e. the coupling energy per unit area E_c in Eq. (3), can be determined by varying the magnetic field applied to the trilayer structure and measuring the BLS spectra or MOKE magnetization curves [54]. These optical techniques have increased the sensitivity to the overlayer as compared to conventional magnetometry where the signal from the much larger Fe whisker would overwhelm that from the thin Fe overlayer. By assuming that the form of Eq. (3) holds, the BLS measurements allow the separation of $\bar{J}_1$ and $\bar{J}_2$ when the coupling is antiferromagnetic [54]. The bilinear and biquadratic coupling strengths, $\bar{J}_1$ and $\bar{J}_2$, of an optimally grown trilayer are shown in Fig. 10 taken from Heinrich et al. [36]. The separation at 10 and 12 layers in Fig. 10, where the coupling is ferromagnetic, was made assuming that $\bar{J}_2$ was the same as for 9, 11, and 13 layers. The coupling strength was reported to be very sensitive to slight differences in sample fabrication conditions [36,54].

With increasing Cr thickness, $\bar{J}_1$ changes from ferromagnetic to antiferromagnetic at four layers and oscillates around an antiferromagnetic offset until the short-period coupling increases and there is a crossover to ferromagnetic coupling at the 10th layer, with oscillating sign of the coupling after that. Even though the polarization profile P(Fe) of Fig. 7b looks tantalizingly similar to the strength measurements of Fig. 10, P(Fe) is proportional not to the bilinear coupling strength but to M_x of the top Fe layer. The fact that P(Fe) does not saturate suggests a biquadratic component nearly equal to the bilinear coupling. On the other hand, BLS measurements find $|\bar{J}_1| > 2|\bar{J}_2|$, except near zero crossings of $\bar{J}_1$, and the coupling is not canted but collinear, either ferromagnetic or antiferromagnetic [36]. We attribute this discrepancy between these BLS measurements and the SEMPA measurements of Fig. 7 to slightly rougher Cr in the Fe/Cr_{wedge}/Fe trilayer as indicated by the less than optimal RHEED oscillations in Fig. 7c.

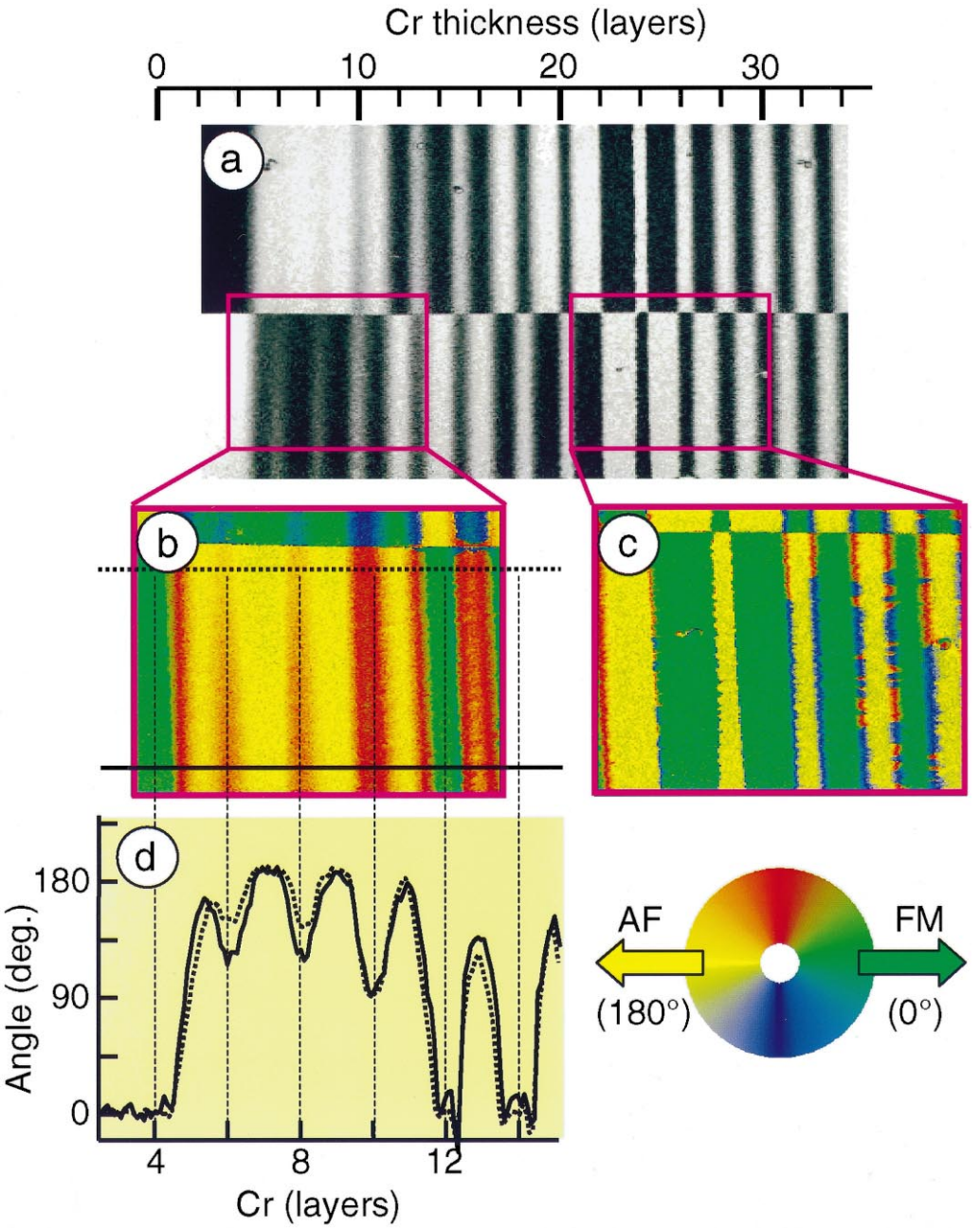

Fig. 9. (a) SEMPA image showing the oscillatory magnetic coupling in an Fe/Cr_{wedge}/Fe(0 0 1) trilayer. (b) and (c) Enlarged angle maps from the regions outlined in (a). The colors give the direction of the magnetization. Canted non-collinear coupling is evident in (b). 90° biquadratic coupling regions, shown as red and blue, of varying width are seen in (c). (d) There is some variation of the canted coupling as seen in the line scans at two positions across the whisker.

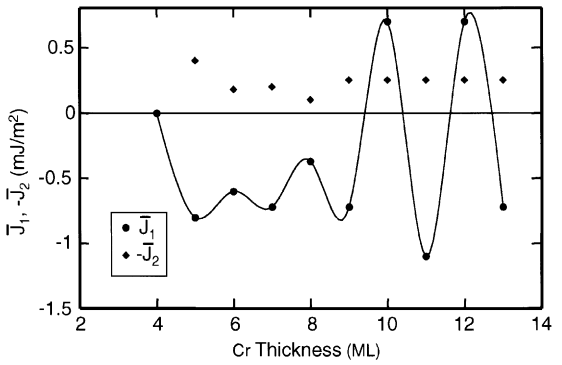

Fig. 10. BLS measurements of bilinear $\bar{J}_1$ and the biquadratic $-\bar{J}_2$ coupling in optimally fabricated Fe/Cr/Fe(0 0 1) trilayers as a function of Cr thickness [36].

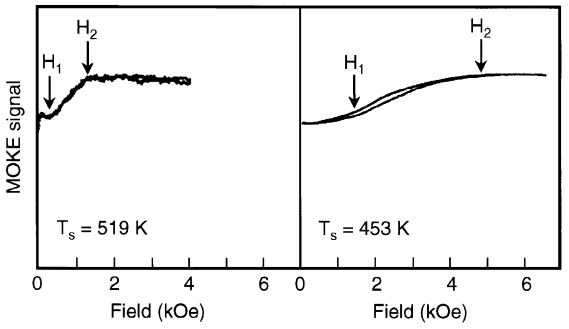

Fig. 11. MOKE signal proportional to magnetization versus magnetic field for two Fe(20 ML)/Cr(11 ML)/Fe(0 0 1) whisker trilayers. The increase in H_1 and H_2 indicate a larger bilinear coupling strength $\bar{J}_1$ in the sample shown on the right for which the first ML of Cr was deposited at a substrate temperature of 453 K and subsequent layers at $T_{s,opt}$ compared to the other trilayer shown on the left for which the first 7 ML of Cr were deposited at 519 K and the remaining layers at $T_{s,opt}$ [42].

The coupling strength shown in Fig. 10 measured from optimum samples is still over an order of magnitude smaller than predicted theoretically [55,56]. The sensitivity of the coupling strength to the substrate temperature during the deposition of the first few Cr layers suggests that it is affected by interfacial alloying. An indication that interface alloying affects the coupling strength is seen from the very different H_1 and H_2 in Fig. 11 for samples grown at different temperatures [42]. For applied fields slightly above H_2, the magnetic moments in the Fe whisker and the Fe overlayer are parallel. For fields slightly below H_1 the overlayer and whisker moments are antiparallel [36]. A decrease in $\bar{J}_1$ by a factor of three from -1.23 to -0.41 mJ/m^2 was calculated from the hysteresis curves when the interface was formed at substrate temperatures of 453 and 519 K, respectively, and the rest of each Cr film was deposited at $T_{s,opt}$ [42].

There are limits on how much the substrate temperature during interface formation can be reduced to decrease the effect of alloying on the coupling strength. A substrate temperature of at least 370 K was found to be necessary to obtain reasonable growth [36]. Even with this care taken to minimize interfacial alloying, these samples showed the reversed phase of the oscillations in the thinner Cr regions. As seen in the SEMPA measurements, antiferromagnetic coupling is present for an odd number of Cr layers instead of the ferromagnetic coupling for an odd number of Cr layers as expected for perfect antiferromagnetic stacking. Heinrich et al. also induced variations in the coupling strength by depositing 1–3 ML of Cu, Ag, or Mn at one of the Fe–Cr interfaces [36]. The results were compared to recent calculations [57], but further discussion here is beyond the scope of this paper.

Atomic-scale defects, for example due to interfacial alloying or steps, cause diffuse scattering of electron states and cause frustration. These effects tend to reduce the coupling for each discrete thickness, $J_1(n)$. This discrete thickness coupling strength is used to determine the biquadratic coupling strength, Eq. (6), and the lateral response length l. While the steps that cause the thickness fluctuations also lead to diffuse scattering and frustration, in general, they have a more important effect. The thickness fluctuations average the coupling at discrete thicknesses over the growth front to give a reduced average coupling strength $\bar{J}_1(t)$, Eq. (5). This averaging explains the reduced coupling strength in systems like Fe/Au where no alloying is believed to occur [12]. The thickness fluctuations also cause the biquadratic coupling in the conventional model. In contrast, the interfacial alloying occurs on a lateral length scale of atomic dimensions (see Fig. 5a) and only affects $\bar{J}_2$ indirectly through the effect of diffuse scattering on $J_S(n)$.

The critical fields in Fig. 11 are determined from fitting the hysteresis curves in the conventional model taking into account the micromagnetic response of the Fe whisker as well as the Fe overlayer [28]. The antiferromagnetic alignment of the Fe films is expected to show a jump at H_1 and a well-defined kink at H_2. The remanence observed in Fig. 11 is that of the Fe whisker. Heinrich et al. [36] argue that a variation in exchange coupling strengths $\bar{J}_1$ and $\bar{J}_2$ by $\pm 10\%$ over length scales larger than the lateral response length is sufficient to explain the rounding of the hysteresis curves as well as the differences between H_1 and H_2 determined by BLS and MOKE on the same samples. The hysteresis curves can be explained in the conventional model.

The variation of the coupling strength out to thicker Cr layers is shown in Fig. 12a for an Au(10 ML)/Fe(15 ML)/Cr_{wedge}/Fe whisker sample. The first two layers of the wedge were grown at 403 ± 10 K and the rest at 623 ± 20 K. This figure is a series of MOKE images, each acquired at a different applied field [53]. The dark vertical bands are the antiferromagnetically coupled regions that switch at different applied fields. For this 15 layer Fe film, switching the magnetization from antiferromagnetic to ferromagnetic in an applied field of 100 kA/m corresponds to a coupling strength $\bar{J}_1$ of 0.47 mJ/m^2. At a Cr thickness of 11 layers and below, the field available in these experiments was insufficient to switch the Fe. The interpretation of the fading contrast of the antiferromagnetic peaks at Cr thicknesses of 13 and 15 ML would require a measurement of the hysteresis loops at these points. Possible explanations include either a distribution of coupling strengths or the slow approach to saturation expected from the torsion model. This series of images graphically shows how the exchange coupling depends on Cr thickness with a clear minimum at the phase slip for a Cr thickness of 24–25 layers.

It is also possible from SEMPA data to get some idea of the variation of the strength of the biquadratic coupling $\bar{J}_2$ from the width of the transition region between thicknesses of opposite bilinear coupling as was seen in the M_x image in Fig. 9c. In samples, like wedges, where the thickness of the spacer layer varies continuously, there are

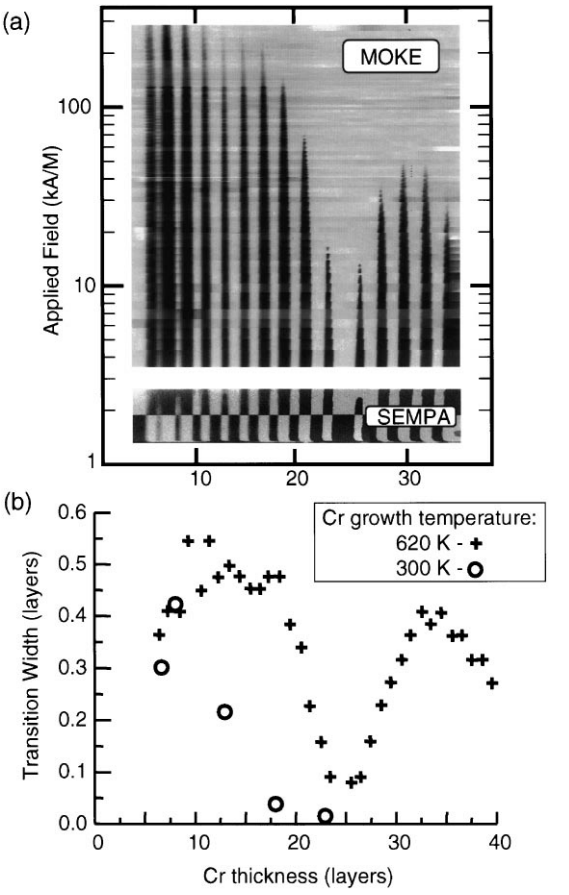

Fig. 12. (a) A series of MOKE images from an Au(10 ML)/Fe(15 ML)/Cr_{wedge}/Fe(0 0 1) whisker taken at various applied magnetic fields showing the field dependence and Cr thickness dependence of the reversal of the antiferromagnetic regions (dark bands). Below 11 ML the field is insufficient to switch the antiferromagnetic regions. The exchange coupling strength, proportional to the switching field, reaches a minimum at the thickness of the phase slip, 24–25 ML. An SEMPA image of the same trilayer at zero applied field is shown at the bottom for reference. (b) The transition width, i.e., the range of Cr thickness where biquadratic coupling is observed when the bilinear coupling goes through zero, is seen to be a minimum at the phase slip where the short-period bilinear coupling is minimum. Data are presented for two Fe/Cr_{wedge}/Fe trilayers: (1) one with the Cr grown at 620 K where the short-period coupling dominates, and (2) one with the Cr grown at RT where the long-period coupling dominates.

transition regions where the averaged bilinear coupling, $\bar{J}_1(t)$, changes from ferromagnetic to antiferromagnetic going through zero. In these transition regions, the biquadratic coupling, $\bar{J}_2$, becomes

larger than $\bar{J}_1(t)/2$, and the minimum energy configuration for the Fe magnetizations is non-collinear. The width of this transition region is the distance between the points where $\bar{J}_1(t) = 2\bar{J}_2$, and $\bar{J}_1(t) = -2\bar{J}_2$. In Fe/Cr multilayers, the unaveraged short-period coupling is larger than the unaveraged long-period coupling, so the strength of the biquadratic coupling is proportional to the square of the change in the short-period coupling strength from one layer to the next, see Eq. (6), $\bar{J}_2 \propto (\Delta J_S)^2$. This dependence is independent of whether thickness fluctuations obscure the short-period coupling from $\bar{J}_1(t)$ or not. The constant of proportionality will vary with the interface quality, represented in Eq. (6) by the terrace length L. Near the thickness t_0 where the coupling changes sign, the averaged bilinear coupling varies as $\bar{J}_1(t) \propto J_1'(t - t_0)$. Thus we expect the transition width to vary like $w \propto (\Delta J_S)^2/J_1'$. Near a phase slip in the short-period coupling, the envelope of the unaveraged short-period coupling goes through zero linearly, $\Delta J_S \propto (t - t_{slip})$. As it does, the biquadratic coupling goes through zero. Based on the simple arguments presented here, we would expect to see the width of the transition region, w, go to zero near the phase slip either linearly if the short-period coupling survives the thickness fluctuations or quadratically if it does not. The results in Fig. 12b are consistent with these expectations, but insufficient for a quantitative comparison to the model.

6. Optimal trilayer structures: interpretation

In principle, a perfect multilayer structure composed of thin Fe and Cr films results in a coherent structure with one thermodynamic phase transition for the whole structure at a temperature between the Curie temperature of bulk Fe and the Néel temperature of bulk Cr [58]. In the multilayer, we expect the Fe to induce antiferromagnetic order in the Cr up to the transition temperature of the multilayer. The degree of order in the Cr depends on the temperature, the Cr thickness, and the distance from the interface. When the Cr becomes thick enough, we expect it to behave as if it had a transition at the bulk Néel temperature even though the transition is broadened and not a true thermodynamic phase transition [58]. The coupling can be understood as the response of the Fe atoms at one interface to the electrons in the Cr spacer that are polarized by the magnetized states in the other Fe layer. This description also applies for paramagnetic spacer layers. There, the Fe induces a (weak) spin density that mediates the coupling.

A paramagnetic description of Cr was the basis of the RKKY-like calculation used by Wang et al. [59,60] to treat the magnetic coupling in Fe/Cr/Fe. The striking feature of the calculation was the short-period oscillatory coupling with a period given by the Fermi surface nesting vector $\boldsymbol{Q}$ of the paramagnetic Fermi surface shown in Fig. 1. At the time of the calculation, only the long-period coupling oscillations had been observed [4] and Wang et al. [59,60] showed how interface roughness could average out the short-period oscillations and bring their results into better agreement with that experiment.

The conventional model, which includes such an RKKY calculation, treats Cr in an itinerant electron or band picture and ignores the electron–electron interactions in the Cr that stabilize the antiferromagnetic state. At the other extreme is the localized moment picture in which atomic Cr moments are antiferromagnetically coupled by a Heisenberg exchange. The proximity model [23] of Eq. (7) is of this type. These models do not describe the Cr incommensurate spin density wave. Between these extremes are calculations based on different models for treating the electron–electron interactions. Examples include calculations such as those of Mirbt et al. [55] and of van Schilfgaarde and Herman [56] based on the local spin density approximation, calculations of the Strasbourg group [61] based on the tight binding approximation and on-site Coulomb interactions, and the calculations of Shi and Fishman [62] based on models for the free energy of bulk Cr in different ordered states. In most calculations, the interlayer exchange coupling is taken as the difference between the calculated energy of the structure for the ferromagnetic layers aligned parallel and the energy for antiparallel alignment. It is possible in local spin density approximation calculations to modify the treatment of the electron–electron

interactions so as to suppress the formation of antiferromagnetism in the Cr. This allows an approximate comparison of the coupling in both paramagnetic and antiferromagnetic SDW Cr. Short-period oscillatory coupling is found in all cases, but the strength varies. At a Cr thickness of 11 ML, corresponding to the maximum coupling measured by Heinrich et al. [36], the strength of the calculated coupling through SDW Cr ranges from approximately 60 to 80 mJ/m^2 and is roughly three times stronger than that calculated for paramagnetic Cr [55,56]. The experimental coupling strength, of order 1 mJ/m^2, is reduced by the interfacial alloying and also, we believe, by Cr thickness fluctuations. These are difficult to avoid even in carefully optimized growth.

In contrast to local magnetic moments of a rare-earth metal or of a conventional antiferromagnet, Cr is an itinerant antiferromagnet with a spin density wave such that ordered magnetic moments at each lattice site can vary in magnitude. Shi and Fishman have presented a model of Fe/Cr/Fe that treats the competition between the SDW antiferromagnetism of the Cr spacer layer and the antiferromagnetic coupling of the Cr and Fe at the interfaces [62]. For ideal interfaces, the interface coupling tends to increase the SDW amplitude at the interfaces whereas the intrinsic antiferromagnetism of the Cr favors the temperature-dependent bulk SDW values for the amplitude and wave vector. When the bulk contribution from the Cr spacer is sufficiently small compared to the interface energies, as is the case for a thin Cr spacer or at higher temperature, Shi and Fishman show that the commensurate SDW (CSDW) is favored over the incommensurate SDW (ISDW) [62,63]. The thickness and temperature dependence of the transition from the commensurate phase with $n = 0$ nodes to the first incommensurate phase with $n = 1$ node in the SDW is shown by the heavy line in Fig. 13 [63]. The variation of the commensurate-to-incommensurate transition with temperature shown by the heavy line in Fig. 13 is consistent with the measured change in the position of the phase slip depicted by the solid line in Fig. 8b. The $n = 1$ to 2 transition in Fig. 13 corresponds to the second phase slip shown by the dashed curve in Fig. 8b. The increased incommensurability of Cr on Fe, indicated by the

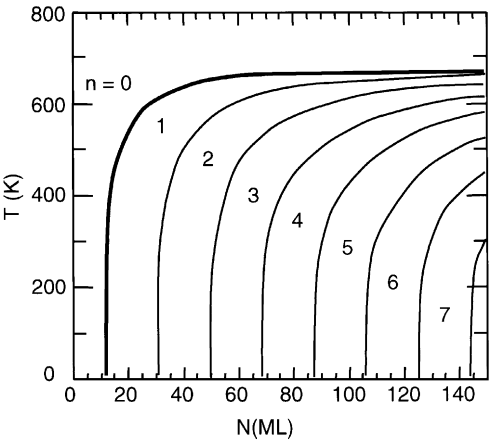

Fig. 13. Calculated [63] curve showing the transition (heavy line) from commensurate order ($n = 0$) to incommensurate order, ISDW with one node ($n = 1$), as a function of temperature and Cr thickness. The lighter curves show the transitions between ISDWs with different number of nodes.

smaller node-to-node distance of 20 ML at 300 K for the $Fe/Cr_{wedge}/Fe$ compared to the 27 ML for bulk Cr as shown in Fig. 8a, is attributed to the 0.6% smaller lattice constant for Cr on Fe than for Cr in the bulk. Using this lattice constant, the model gets the node-to-node distance correct, but the phase slips occur at smaller Cr thicknesses than in experiment.

The SEMPA measurements are not directly sensitive to the presence of antiferromagnetic order in the Cr. However, the qualitative agreement between the model calculation and the measured temperature dependence of the phase slips is strong evidence that the Cr layer in these experiments is in an antiferromagnetic state. Within the conventional model, the change in the phase slip would have to come from the temperature dependence of the Fermi surface. However, the temperature dependence of the Cr Fermi surface is too weak to give the observed variation in the incommensurability. The agreement also implies that the antiferromagnetic order that exists well above the bulk Néel temperature of Cr is due to the proximity of the Fe.

Also in accord with the model of Shi and Fishman [62] is the fact that the coupling strength in Fig. 12a decreases with Cr thickness up to the phase slip at the node in the SDW at a Cr thickness

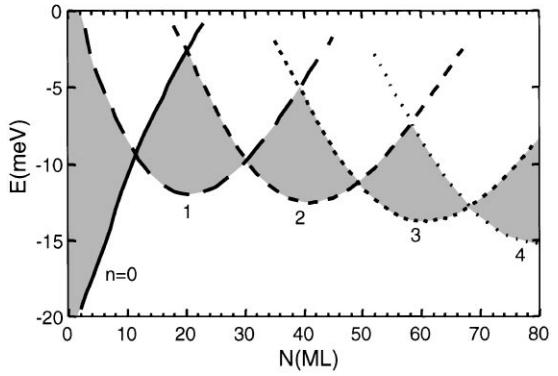

Fig. 14. The energy of a spin density wave in Cr with 0, 1, 2, 3, or 4 nodes as a function of Cr thickness calculated for a temperature of 100 K [64]. The boundaries of the shaded regions show the variation of the coupling strength.

of 24–25 layers and then increases again. The family of curves in Fig. 14 gives the energy of a spin density wave in Cr for $n = 0$, 1, 2, or 3 nodes, calculated with the same model parameters as Fig. 13 [64]. The ground state of a trilayer is commensurate with alternating ferromagnetic and antiferromagnetic alignment of the Fe films up to a thickness where the $n = 0$ and 1 lines cross. After this point the ground state has incommensurate SDW order. The phase slip occurs at the crossover where the two types of SDW have the same energy. In the region of the commensurate SDW, reversing the orientation of the Fe layers from the low-energy configuration at a given thickness, introduces a node in the SDW, raising the energy to that given by the $n = 1$ curve. The coupling energy of the system, $E_{AF} - E_F$, is just the difference between the two curves that form the boundary of the shaded area. This gives the envelope of the coupling strength in this model. Comparing Fig. 12a and Fig. 14 shows that this result is in qualitative agreement with what is measured.

With this overall picture of the short-period coupling in place, we will now discuss the inevitable magnetic frustration at imperfect interfaces. Steps in the Fe whisker substrate and roughness at the upper Fe–Cr interface due to the Cr growth lead to frustration that is likely relieved in two different ways. We first consider frustration due to steps in the whisker substrate. The typical 1 μm step separation on the Fe whisker surface is much larger than the Cr thickness of less than 10 nm. The frustration caused by these Fe steps for a number of complete Cr layers is therefore expected to be taken up in the Cr film as shown in Fig. 3b, rather than as a very long Fe–Cr interface wall as would be required in Fig. 3c. Even for perfect growth on a very flat Fe whisker, at other than a perfectly completed layer, there will be thickness fluctuations in the Cr spacer layer on a length scale L, which is at least an order of magnitude less than the step spacing on the whisker at the growth temperatures used. Over the lateral response length $l(l > L)$ that it takes the Fe magnetization in the overlayer to change direction, the Fe overlayer responds to the average of the coupling strengths for each Cr thickness as in Eq. (5). The magnetization of the Fe overlayer is constant. This causes the frustration at the Cr–Fe overlayer interface that is likely relieved by an interface wall of the type shown in Fig. 3c.

One possible consequence of such frustration is canted coupling as is often observed for the thin part of the Cr wedge, as seen in Fig. 9b for example. A plausible explanation of the results can be given in terms of Slonczewski's fluctuation model [31]. The angle of the coupling comes from the competition between $\bar{J}_1$ and $\bar{J}_2$, see Eq. (3), which is highly sensitive to sample properties. The decrease of the biquadratic coupling relative to the short-period bilinear coupling after a dozen or so layers can be understood from Eq. (6). The biquadratic coupling decreases as the square of the bilinear coupling, so it decreases faster than the bilinear coupling as the latter decreases. In the thicker parts of the Cr wedge, the thickness fluctuation model of biquadratic coupling explains the 90° coupling in the transition regions where the averaged bilinear coupling, $\bar{J}_1(t)$, changes from ferromagnetic to antiferromagnetic going through zero.

In summary, the magnetic coupling in optimized Fe whisker trilayers can be described by Eq. (3) where the bilinear coupling consists of a short-period oscillatory coupling that dominates the long-period coupling. To correctly explain the short-period coupling, it is necessary to go beyond the conventional model and include a treatment of the electron–electron interactions of the type that stabilize the incommensurate order in Cr. The

observed non-collinear coupling can be explained satisfactorily by the Slonczewski thickness fluctuation model [31]. Agreement with the trends of that model does not imply that other models may not be developed that give better descriptions of the non-collinear coupling; in fact, the best description may change with the Cr thickness.

7. Trilayers with varying interfacial roughness: measurement

The degree of interface roughness in Fe/Cr/Fe trilayers has a very strong influence on the magnetic coupling. The roughness of a Cr spacer layer grown on an Fe whisker substrate is very dependent on the temperature of the substrate during evaporation of the Cr [5,36,48]. A GaAs(0 0 1) substrate with an Ag buffer layer has also been used for the epitaxial growth of Fe/Cr/Fe trilayers which exhibit long- and short-period oscillations in the magnetic coupling [65–69].

We discuss the similarities and differences in the Fe whisker and GaAs-based trilayers with regard to both the interface structure and the magnetic coupling. Results will first be presented for Fe whisker trilayers with varying degrees of interfacial roughness caused by different Cr growth temperatures. We then discuss the results from the GaAs-based trilayers. STM measurements of the roughness and mean island separation are discussed for both types of samples and summarized in Table 2.

Trilayers grown on Fe whiskers are unique because the interface at the whisker is exceptionally smooth. Because the Fe(0 0 1) whisker surface is very flat, the roughness of the Cr layer determines the thickness fluctuations, i.e., σ_t is assumed equal to σ_{Cr}. STM images of approximately 5 ML Cr films grown on Fe whisker substrates at 323 ± 20 and 488 ± 20 K are shown respectively at the top left and right in Fig. 15a and Fig. 15d [37,48]. The height–height correlation function was computed for each image to obtain the mean island separation R and the rms roughness σ shown at the bottom of Table 2. There is a strong correlation between the growth temperature of the Cr spacer layers and the observed oscillatory coupling in the

Table 2
Interface parameters of Fe/Cr/Fe trilayers. The mean island separation, R, the rms roughness, σ, and the standard deviation of the thickness distribution, σ_t, are given for different films grown at temperatures, T_S, on GaAs and Fe whisker substrates. Note that the roughness measurements of 17.4 ML thick Cr films on GaAs substrates and approximately 5 ML thick Cr films on an Fe whisker cannot be compared directly because roughness increases with thickness. For example, using the power law dependence of σ_{Cr} from a previous analysis [48], one estimates $\sigma_{Cr} = 0.86$ ML for a 17.4 ML Cr film grown at 488 K on an Fe whisker

Notation	Layer	T_S (K)	Interfaces		Spacer layer σ_t (ML)
			R (nm)	σ (ML)	
GaAs substrate, $t_{Cr} = 17.4$ ML					
RT	Top Fe	300	–	–	–
	Cr	300	6.8	1.25	1.94
	Bottom Fe	300	6.1	1.46	–
MT_{570}	Top Fe	520	–	–	–
	Cr	520	22.4	1.32	1.88
	Bottom Fe	100/570	19.7	1.32	–
MT_{520}	Top Fe	520	–	–	–
	Cr	520	15.4	1.11	1.46
	Bottom Fe	100/520	10.1	0.90	–
Fe whisker, $t_{Cr} \approx 5$ ML					
RT	Cr	323	10 ± 0.5	0.86	0.86
Intermediate T	Cr	488	31 ± 1	0.47	0.47
High T	Cr	573	85 ± 10	~ 0	~ 0

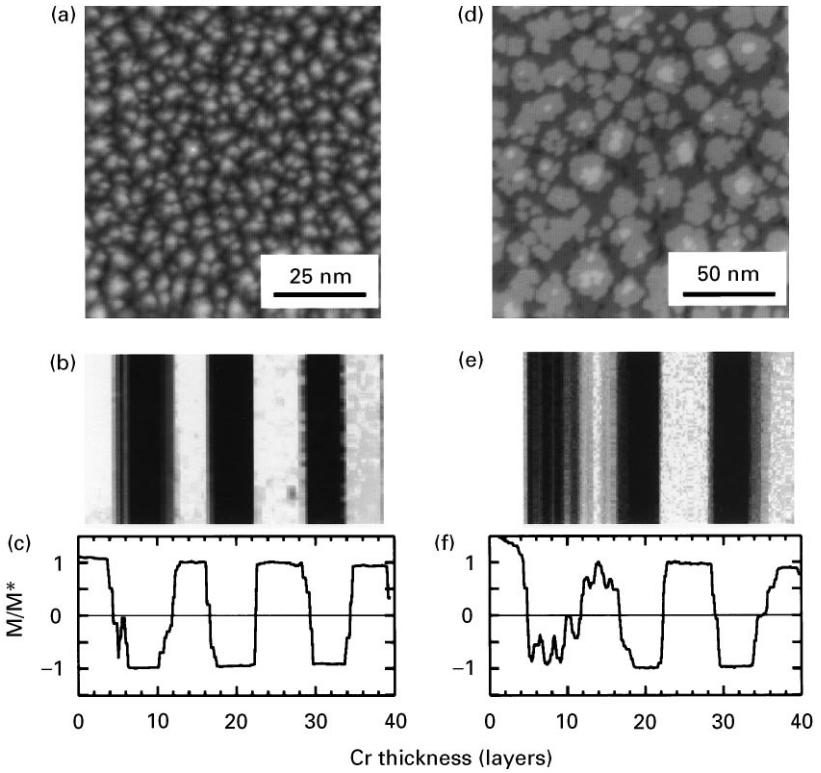

Fig. 15. STM images [48] of approximately 5 ML of Cr grown on an Fe(0 0 1) whisker at temperatures of 323 and 488 K shown in (a) and (d), respectively. Note change in lateral scale. SEMPA images of $Fe/Cr_{wedge}/Fe(0\,0\,1)$ trilayers where the Cr was grown at 303 and 473 K are shown in (b) and (e), respectively. The relative magnetization from SEMPA images of (b) and (e) is shown in (c) and (f), respectively, normalized to the saturation value M^* in a range of Cr thickness from 20 to 30 ML.

rougher trilayers grown on Fe whiskers. The SEMPA image of an Fe/Cr wedge/Fe(0 0 1) trilayer structure grown at 303 ± 10 K and a magnetization profile from this image are shown in Fig. 15b and Fig. 15c respectively. The corresponding figures for the $Fe/Cr_{wedge}/Fe(0\,0\,1)$ grown at 473 ± 10 K are shown in Fig. 15e and Fig. 15f [48]. For the lower temperature growth, the magnetic coupling shows primarily long-period coupling with some fine structure at 6 layers. Although the trilayer with the Cr wedge grown at 473 K exhibits primarily a long-period coupling, short-period oscillations can be observed out to a thickness of 18 Cr layers. As in Fig. 7b and Fig. 9b, the fact that the magnetization does not correspond to complete ferromagnetic or antiferromagnetic alignment, means that there is an M_y component and that the magnetization is canted.

The starting point for trilayer growth on GaAs is a substrate quite different from the Fe whisker. The GaAs-based samples are typically prepared by first depositing a 1 nm Fe seed layer on the GaAs(0 0 1) surface followed by a 150 nm Ag buffer layer, all at 373 K, followed by a 1 h anneal at 573 K. Fe/Cr/Fe trilayers subsequently deposited at 293 K showed long-period oscillations quite similar to those observed for the trilayer grown at RT on the Fe whisker [67]. When the trilayer was deposited at 523 K, except for the first few Fe layers which were deposited at room temperature to minimize diffusion of the Ag into the Fe, short-period oscillations in the coupling strength were observed, but no phase slips [67,68]. The coupling for growth at 523 K exhibited a strong biquadratic component in addition to the bilinear component. At this growth

temperature, a negative (antiferromagnetic) bias of the coupling up to 25 ML Cr was observed, which decreased with increasing measurement temperature [67].

Recently, Schmidt et al. [69] combined a careful STM characterization of trilayers fabricated on Ag-buffered GaAs substrates with measurements of the magnetic coupling strength. The sample preparation differed slightly from those studied by the Grünberg group [67], but the magnetic coupling results are similar. The combination of structural as well as magnetic measurements on these samples makes them of particular interest for closer examination. In samples denoted as room-temperature (RT)

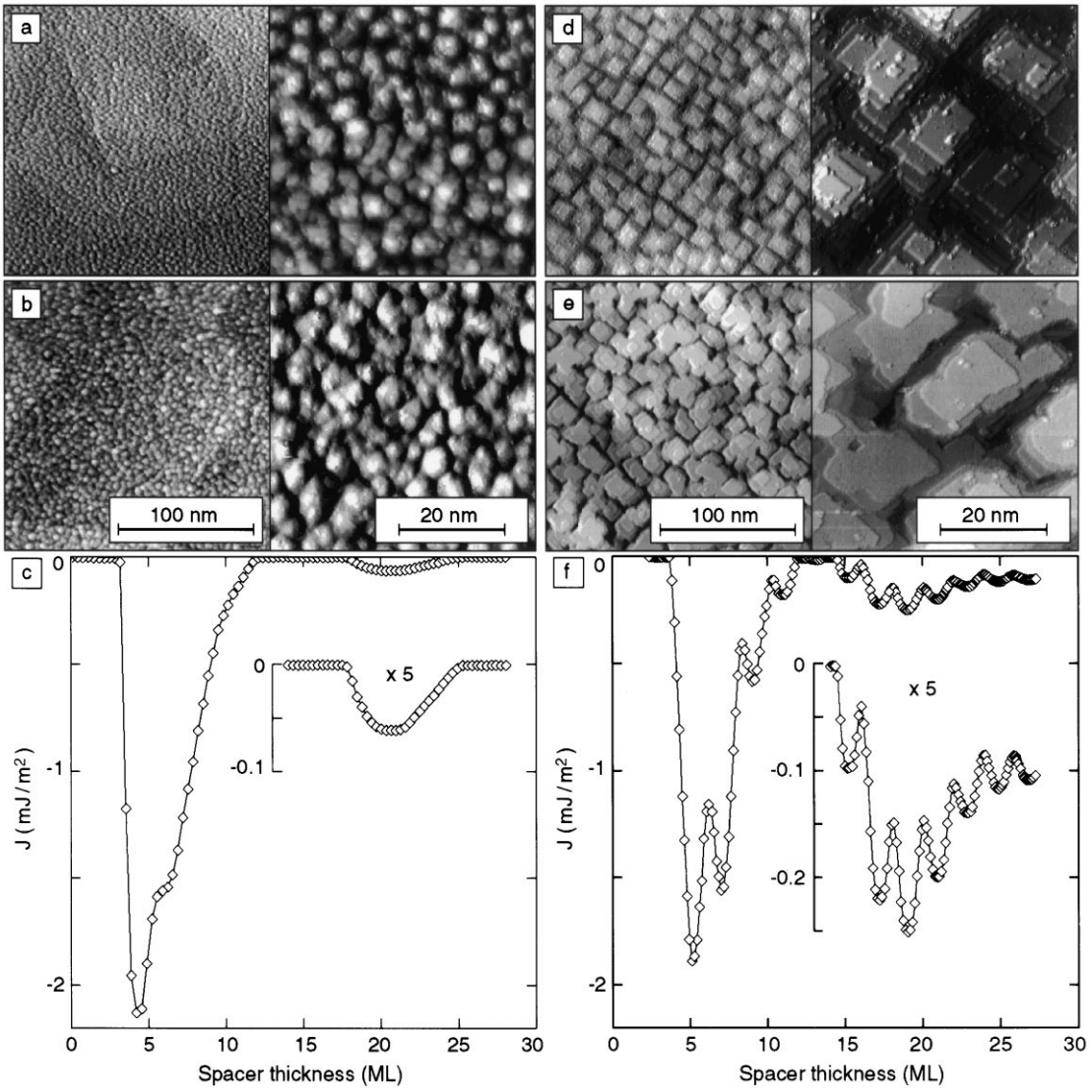

Fig. 16. Structural characterization and magnetic coupling measurements of Fe/Cr_{wedge}/Fe(0 0 1) trilayers grown on Ag-buffered GaAs(0 0 1) [69]. (a) STM overview on left and detail image on right of first Fe layer grown at RT. (b) Similar images of the Cr layer grown at RT at a thickness of 17.4 ML. (c) MOKE measurement of the magnetic coupling showing the long-period oscillatory behavior. (d–f) Similar figures for the MT_{570} trilayer. Short-period oscillations of the coupling are now evident.

samples, the entire trilayer was fabricated at room temperature. A second designation, mixed temperature (MT_T), corresponds to samples where the first 2 nm of the first Fe layer were deposited at 100 K to inhibit segregation of Ag to the surface, and the remaining 3 nm of the 5 nm bottom Fe layer were deposited at temperature T which was 520 or 570 K. The Cr layer and the 5 nm Fe overlayer were both deposited at 520 K. STM images were acquired after deposition of the bottom Fe layer and then again after deposition of the Cr layer.

From the STM images the rms roughness, σ, and mean island separation, R, were calculated. The results are summarized at the top of Table 2. From the inequivalence of R for Fe and Cr and from modeling, Schmidt et al. [69] concluded that the roughness of the Fe bottom layer was not correlated with the roughness at the top of the Cr layer. On the basis of this argument, they calculated the rms thickness fluctuation of the Cr spacer layer, $\sigma_t = (\sigma_{Fe}^2 + \sigma_{Cr}^2)^{1/2}$ also shown in Table 2.

Interesting correlations are found between the magnetic coupling and the growth morphology as characterized by the STM. The STM images and the magnetic coupling results for RT and MT_{570} structures are compared in Fig. 16. Fig. 16a–Fig. 16c show respectively an STM image of the bottom Fe layer, an STM image of the Cr layer at a thickness of 17.4 ML (2.5 nm), and the magnetic coupling curve, determined from MOKE hysteresis loops, for the RT $Fe/Cr_{wedge}/Fe(0\,0\,1)$ trilayer. The STM images include both low- and high-resolution images. Fig. 16d–Fig. 16f contain the corresponding images for the MT_{570} trilayer. The magnetic coupling from the RT trilayer exhibits long-period oscillatory coupling with a hint of structure at a Cr thickness of six layers. The MT_{570} sample shows a long-period oscillation modulated by short-period oscillations. A MOKE hysteresis curve for the MT_{570} sample at a Cr thickness of 17.4 ML is shown in Fig. 17. The plateaus in the magnetization, nearly equal to half the saturation magnetization for zero applied field, are indicative of 90° coupling for this multilayer with Fe layers of equal thickness. In fact, for both mixed temperature (MT) trilayers, biquadratic coupling dominated over most of the thickness range. For 7 ML and below,

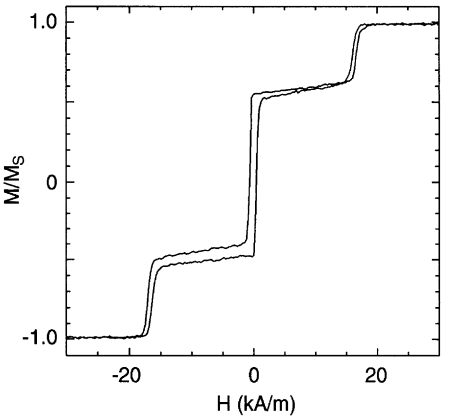

Fig. 17. MOKE hysteresis loop from an MT_{570} trilayer at a Cr spacer-layer thickness of 17.4 ML shows that the magnetic coupling is predominantly biquadratic.

bilinear antiferromagnetic coupling is apparent in the hysteresis curves [70]. In contrast to the MT_{570} samples, the MT_{520} coupling data showed only very weak short-period oscillations.

8. Trilayers with varying interfacial roughness: interpretation

The long-period oscillatory coupling is clearly seen in trilayers on Fe whiskers with the Cr grown at room temperature, Fig. 15b and Fig. 15c, and in trilayers on Ag-buffered GaAs(0 0 1), Fig. 16c. Unlike the short-period coupling that is believed to have its origins in the antiferromagnetism of Cr, we believe the long-period coupling can be described using a quantum well model in the same way as is used to describe the coupling through noble metals. However, even accepting this model, the important part of the Fermi surface is still controversial, as discussed elsewhere in this volume [11]. One proposal is that the appropriate spanning vectors for the long-period oscillatory coupling would be located at the N-centered ellipses in Fig. 1 [71–73]. The critical spanning vectors of the N-centered ellipses are similar for the (0 0 1), (1 1 0) and (2 1 1) interfaces. Since this part of the Fermi surface is not believed to be strongly dependent on the presence or absence of antiferromagnetic order,

the paramagnetic Fermi surface should be appropriate. In this case, the long-period coupling would be expected to be relatively insensitive to temperature and disorder.

When there are sizable thickness fluctuations, as seen in the STM images of Fig. 15a and Fig. 16b, the long-period coupling is observed, because the short-period coupling $\bar{J}_S$ is reduced by thickness fluctuations as described in Eq. (5). An example of the effect of thickness fluctuations on the short-period coupling is shown in Fig. 18a. This plot of the averaged coupling, $\bar{J}_S$, was generated by assuming a coupling J_S oscillating in sign with each one layer change in Cr thickness, and adding together the coupling contributions from all the layers in the growth front. Distributions of the discrete thickness fluctuations were generated with varying standard deviation, σ_t, by sampling Gaussian distributions at integer layer thicknesses and appropriately normalizing the discrete distributions. Similar distributions were found to be a good approximation for rough growth of thin layers of Cr on Fe whiskers [48]. The plot is normalized to 1 for ideal interfaces. For a thickness distribution with a standard deviation $\sigma_t = 1$ ML the value of the normalized $\bar{J}_S$ has decreased to 0.014. As the strength of the averaged short-period coupling becomes weaker than competing energies such as those of the biquadratic coupling, the anisotropy, or the long-period coupling, it will become more difficult to observe.

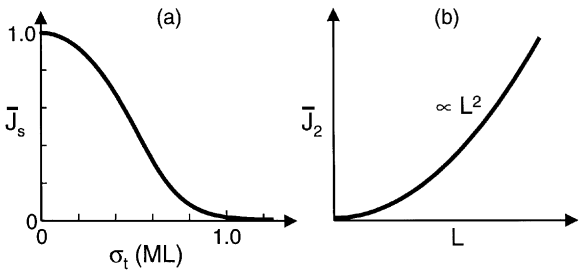

Fig. 18. Model dependence of coupling strengths on structured parameters. (a) The thickness fluctuations (or equivalently the Cr roughness if there is one flat interface at the whisker) reduce the short-period coupling J_S, which alternates in sign with each Cr layer, to $\bar{J}_S$, normalized to one for ideal interfaces, $\sigma_t = 0$. (b) The biquadratic coupling $\bar{J}_2$ varies quadratically with the terrace length L in Slonczewski's thickness fluctuation model, Eq. (6) [31].

For interpreting the magnetic coupling results from trilayers with interfacial roughness, it is useful to keep in mind how different quantities vary with the standard deviation of the thickness distribution, σ_t, and the average terrace length, L. Over the ranges of σ_t and L encountered in the trilayers considered in this section, that is σ_t less than 2 ML and L less than 80 nm, we can say the following: (1) The average long-period coupling strength $\bar{J}_L$ remains nearly constant, (2) the average short-period coupling $\bar{J}_S$ decreases dramatically with increasing σ_t while J_S remains constant, and (3) there is a wide variation in the biquadratic coupling. In the thickness fluctuation model of biquadratic coupling, Eq. (6), $\bar{J}_2$ varies quadratically with the terrace width L as shown in Fig. 18b.

We call attention to an additional experimental result from RT trilayers on Fe whiskers that places constraints on models of biquadratic coupling. In these samples, L is small giving a relatively small $\bar{J}_2$, but biquadratic coupling is still observed when the long-period coupling goes through zero. This can be understood in terms of the thickness fluctuation model of biquadratic coupling; even though average short-period coupling $\bar{J}_S$ is small for low-temperature growth, it is the unaveraged J_S, which is not small, that contributes to the biquadratic coupling. This idea is supported by the fact that the widths of the biquadratic coupling regions from an SEMPA image, see Fig. 12, are smallest where J_S is at a minimum in the vicinity of the phase slips in the short-period coupling.

A significant feature of the magnetic coupling in the Fe whisker trilayer which we want to be able to explain is the canted biquadratic coupling observed up to a Cr thickness of 18 ML in Fig. 15f. Unlike optimal trilayers on Fe whiskers where the short-period bilinear oscillations dominate for Cr thicker than about 10 ML, for Cr growth on whiskers at 488 K the short-period coupling is much reduced. The canted coupling can be interpreted as a competition between biquadratic and bilinear coupling. The variation in the canted coupling with Cr thickness can be understood in the thickness fluctuation model of biquadratic coupling. The canted coupling dies out above about 18 ML Cr thickness because, as interface roughness and thickness fluctuations increase

with Cr thickness, L decreases, and thus the biquadratic coupling $\bar{J}_2$ decreases.

Turning to the trilayers on GaAs substrates [69], Table 2 shows that the roughness of the Cr grown at room temperature and at 520 K in the MT_{570} sample is about the same. However, the mean island spacing R is much larger for high-temperature growth, as also can be seen by comparing the STM images in Fig. 16b and Fig. 16e. The magnetic coupling is clearly very different. The striking STM images of the MT_{570} Fe and Cr surfaces show mesa-like structures with deep canyons between. This morphology is thought to result from relieving the strain in the Fe film grown on Ag with a 0.8% lattice mismatch. Similar structure is seen in the Cr growth, but the mean island spacing R increases over that of the Fe film by 52 and 14% for the MT_{520} and the MT_{570} samples, respectively. It is difficult to analyze these results in terms of R, σ and σ_t that we have used to analyze other results because these three parameters do not describe all of the important properties of this morphology. The canyons between the mesas dominate the measured roughness. The height distribution of the mesas alone has a much smaller σ than the surface as a whole. Also, the average terrace length L on the mesas is much larger than the average L derived from R/σ.

Schmidt et al. [69] recognized that it is not possible to understand the coupling strengths of the Fe/Cr/Fe trilayers on GaAs only in terms of the measured σ_t of the thickness distribution as was possible for the SEMPA data from trilayers on whiskers [48]. The largest areas over which the top and bottom interfaces of the Cr film are flat, i.e., regions of constant Cr thickness, called pillars in the model of Schmidt et al., are found in the mesa regions. Regions of constant thickness with a large L contribute most strongly to the biquadratic coupling. These regions may also dominate the short-period coupling, if there is an imbalance of the area associated with pillars of an odd rather than even number of Cr layers. Such an imbalance would be possible if the thickness of these regions is distributed with a σ_t that is much smaller than the σ_t of the whole spacer layer. Schmidt et al. emphasized the importance of the pillar size [69]. From their analysis, they concluded that even for the mesas, the thickness fluctuations were very similar for the MT_{570} sample and the MT_{520} sample. The MT_{570} exhibited short-period oscillations in the coupling that were four times larger than those of the MT_{520} sample. This correlates with the higher proportion of pillars with a large cross section and with the larger R for the MT_{570} sample.

In summary, the magnetic coupling appears quite similar for the rougher RT Cr growth on either the Fe whiskers or the Ag-buffered GaAs. There is long-period oscillatory bilinear coupling in both cases. For higher temperature Cr growth, the observed magnetic coupling is different for trilayers on Fe whiskers and on Ag-buffered GaAs. Both types of samples probably have contributions from both long- and short-period bilinear coupling as well as biquadratic coupling. For Cr growth at 488 K on the Fe whisker, the long-period bilinear coupling dominates with short-period, non-collinear oscillations, up to a Cr thickness of 18 ML, due to the short-period coupling and the biquadratic coupling. For Cr growth at 520 K on the GaAs, above a Cr thickness of 7 ML, the biquadratic coupling dominates [70]. The origin of this difference lies in the structural differences at the interfaces as observed by STM.

9. Fe/Cr superlattices: measurements

The magnetic ordering within the Cr layers and the interlayer coupling in Fe/Cr superlattices is complex and sensitive to interfacial roughness. Neutron scattering has been applied to the study of Fe/Cr multilayers in part because it is directly sensitive to the magnetic order. Neutron scattering at small angles, referred to as neutron reflectivity, is sensitive to magnetic structure on length scales of a few nm, such as a superlattice period. For example, neutron reflectivity distinguishes between ferromagnetic and antiferromagnetic ordering of the Fe layers in Fe/Cr superlattices. Neutron scattering at high angles, referred to as neutron diffraction, is sensitive to magnetic structure on an atomic length scale such as the antiferromagnetic ordering of the Cr moments. Additionally, using incident polarized neutrons and polarization analysis, it is possible to determine the orientation of the moments in the plane of the layer. However, neutron

scattering requires large samples, in particular, superlattices. Since these structures are grown thicker and with more interfaces than the trilayers discussed in the preceeding sections, they tend to have more disorder.

Two groups have carried out most of the neutron scattering investigations of Fe/Cr superlattices. We first review magnetic coupling, transport, and neutron scattering measurements of Fullerton and coworkers as a function of temperature on a series of superlattices differing in the thickness of the Cr layers. The superlattices were epitaxially deposited at temperatures from 350 to 450 K on a 10 nm Cr buffer on MgO(0 0 1) by DC magnetron sputtering [74,75]. Long-period oscillatory coupling was observed up to a Cr layer thickness of 45 ML in saturation magnetization measurements at room temperature and magnetoresistance measurements at room temperature and 4.2 K. For larger Cr thicknesses, biquadratic coupling was observed. The biquadratic coupling in an $[Fe(10\,ML)Cr(51\,ML)]_{20}$ superlattice was characterized in detail by polarized neutron reflectivity (PNR), magnetization and magnetotransport measurements [75,76]. Below the transition temperature for this thickness, $T_N = 187$ K, the biquadratic coupling was not found and the Fe layers became decoupled. We note in passing that in a set of magnetization and magnetoresistance experiments with a Cr(2 1 1) spacer carried out in parallel to those measurements with the Cr(0 0 1) spacer, the same phase, period and strength was found for the long-period oscillatory coupling thereby adding an important constraint on theoretical explanations of the long-period coupling [74,77].

Anomalies in the resistivity and in magnetic properties were used to determine a transition temperature T_I as a function of the thickness of the Cr spacer with a series of Fe(10 ML)/Cr(t_{Cr}) superlattices [76]. The transition temperature is plotted as the solid line in Fig. 19, which shows Cr order as a function of Cr thickness and temperature. Antiferromagnetic order was not observed for $t_{Cr} <$ 29 ML. Above this thickness, T_I rises rapidly and then asymptotically approaches the value for thick films. The temperature T_I was originally attributed to a transition from an ordered incommensurate state to a paramagnetic state [76]. Resistivity

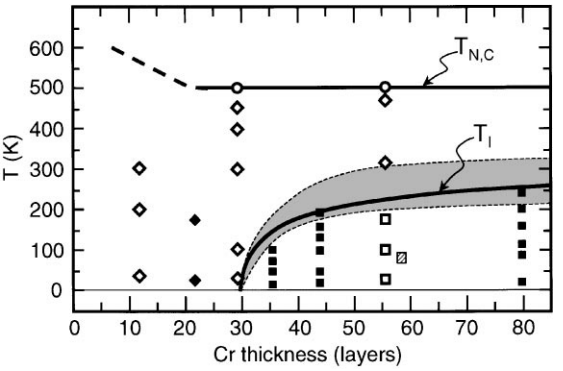

Fig. 19. A phase diagram summarizing the magnetic structure of the Cr spacer layers as a function of temperature and Cr thickness for the measurements on superlattices discussed in the text. The boundary T_I is from transport measurements of Fullerton et al. [76]. Diamonds denote CSDW, squares denote ISDW, and circles denote paramagnetic regions. The measurements are from Fullerton et al. [78] (solid symbols), Schreyer et al. [81,83,84] (open symbols), and Meersschaut [88] (cross-hatch symbol). The shaded region is the transition region found by Schreyer et al. [83]. The rise of the $T_{N,C}$ boundary at smaller Cr thickness (dashed line) was found in recent measurements [86].

anomalies like those measured for the superlattice are seen at the Néel temperature in bulk Cr. In some dilute alloys of Cr, there are similar resistance anomalies associated with transitions from incommensurate to commensurate states. This type of transition was observed by subsequent neutron scattering measurements as discussed below. We label the transition T_I to indicate loss of incommensurate order.

The neutron diffraction measurements for Cr thicknesses greater than about 30 ML and for temperatures below T_I, as determined from the resistivity anomaly, confirmed that the Cr has an incommensurate transverse SDW with $\boldsymbol{Q}$ perpendicular to the interfaces [78]. The ISDW period was independent of Cr thickness and near that of the bulk Cr ISDW. The best fit to the data was obtained assuming that the nodes in the ISDW were near the superlattice interfaces. The scattered neutron intensity for a superlattice with Cr layer thickness of 21 ML, although weak, could be quantitatively fit assuming commensurate antiferromagnetic order [78]. The results for superlattices

on MgO are summarized on the phase diagram of Fig. 19. Fullerton et al. [76,78,79] extensively discussed how the magnetic frustration at rough interfaces could cause the observed behavior as we examine further below.

Schreyer and coworkers investigated the magnetic state of Cr and the magnetic coupling in superlattices grown on two different types of substrates: (1) Fe/Cr superlattices were grown by molecular beam epitaxy (MBE) on Ag-buffered GaAs at room temperature and at 523 K in the same way as for the trilayers [67,80,81] and (2) Fe/Cr superlattices were grown by MBE at 570 K on Cr(0 0 1)/Nb(0 0 1)/ $Al_20_3(1\ \bar{1}\ 0\ 2)$ as described elsewhere [82,83].

The superlattices grown on Ag-buffered GaAs(0 0 1) had relatively few bilayer repeats. The superlattices, $[Fe(36\ ML)/Cr(6\ ML)]_5$ and $[Fe(36\ ML)/Cr(12\ ML)]_9$, were grown at room temperature and 523 K, respectively. X-ray diffraction showed similar correlated roughness for both superlattice types, presumably due to the starting Ag buffer layer surface. At a given growth temperature, uncorrelated roughness, which affects the coupling, was found to increase with an increasing number of layers in the superlattice. The estimated terrace lengths were much smaller for the growth of Cr at RT than at 523 K. For this reason, the bulk of the neutron scattering measurements were done on the superlattices grown at the higher temperature.

From polarized neutron reflectivity measurements, Schreyer et al. [81] found collinear ferromagnetic coupling for the RT superlattice consistent with the RT trilayer results of Grünberg et al. [66]. However, for the 523 K superlattice, PNR measurements at 297, 200 and 42 K showed that the coupling of the Fe layers was non-collinear and at an angle of $50 \pm 4^\circ$ near remanence [80,81,84]. The data points representing this non-collinear coupling, which was associated with commensurate antiferromagnetic order in Cr, are included in Fig. 19. For this superlattice with Fe layers of equal thickness, the observed non-zero remanence and high saturation field indicate non-collinear coupling [81]. The occurrence of the non-collinear coupling is correlated with long terrace lengths (as opposed to short terrace lengths for RT growth) found for superlattice growth at elevated temperatures [80,81,85].

Two transition temperatures were identified when PNR studies were carried out over an extended temperature range for two superlattices, $[Fe(14\ ML)/Cr(56\ ML)]_{133}$ and $[Fe(13\ ML)/Cr(29\ ML)]_{200}$, grown on Al_2O_3 substrates [83]. For a Cr thickness of 56 ML, ISDW order was found for low temperatures. From 175 to 310 K a gradual transition was observed that was characterized by a superposition of a double-peak ISDW spectrum and a single-peak CSDW spectrum of changing relative weight [86]. Finally, at still higher temperatures, a transition to paramagnetic Cr is observed at $T_{N,C}$. These two transitions are distinguished in Fig. 19, the transition from paramagnetic to CSDW Cr that takes place at $T_{N,C}$, and the transition from CSDW to ISDW order that takes place in the shaded region around T_I.

For the superlattice with 29 ML Cr, small-angle PNR and magnetization measurements found non-collinear ordering of the Fe layers below $T_{N,C}$. Additionally, using high-angle neutron diffraction, a modulation of the commensurate antiferromagnetic structure of Cr was observed with a period twice the superlattice period caused by a spiral-type modulation of the Cr layers [83]. The non-collinear coupling of the Fe layers was thus associated with the spiral antiferromagnetic order of the Cr layers. Above $T_{N,C}$ where the long-range Cr order vanishes, MOKE hysteresis loops showed that the Fe layers were no longer coupled [83]. For thin Cr layers, $T_{N,C}$ increases due to the larger influence of the proximity of the Fe on the Cr layer.

Perturbed angular correlation spectroscopy (PACS) measurements have been used to determine the direction of the Cr moments and indirectly the direction of $\boldsymbol{Q}$. In early measurements of superlattices grown by MBE on MgO at 420 K (in contrast to the sputtered superlattices of Fullerton et al. [74]), the Cr was found to be non-magnetic for thicknesses below 42 ML [87]. When the superlattice Cr layers were thicker than 42 ML, Meersschaut et al. [87] found a longitudinal ISDW with the Cr moments out of the film plane, that is the Cr moments were found to be perpendicular to the Fe moments. Recently, the experiments have been repeated on an $[Fe(12\ ML)/Cr(58\ ML)]_{10}$

superlattice grown at 580 K [88]. The behavior of the resistivity anomaly and hysteresis curves for this superlattice were measured and found to be similar to the work of Fullerton et al. [76]. Above the transition temperature $T_I = 200 \pm 10$ K, identified by the resistivity anomaly, the hysteresis curve gave evidence of biquadratic coupling. At lower temperatures the Fe layers were uncoupled. Also in these samples, in contrast to the samples grown at 420 K, PACS measurements at 77 K [88] showed in-plane Cr moments corresponding to a transverse ISDW fitting onto the phase diagram, Fig. 19, of the neutron measurements. This is a striking demonstration that the growth conditions are decisive in determining the magnetic ordering of the Cr in Fe/Cr superlattices. It would be very interesting to know what structural changes in the superlattice were caused by the 160 K increase in Fe/Cr growth temperature.

There are a few remaining discrepancies in the neutron and PACS measurements of the magnetic order of the Cr layers in Fe/Cr superlattices grown at elevated temperatures as summarized in Fig. 19. PACS measurements have yet to report other than paramagnetic Cr below a Cr thickness of 42 ML [87,88]. In this thickness region, neutron measurements of superlattices on Al_2O_3 show that the Cr is in a commensurate spiral state that leads to non-collinear coupling of the Fe layers [83]. Other neutron measurements are not inconsistent with this. The superlattice on Ag-buffered GaAs did not have sufficient layers to produce a large enough signal to determine the existence of the spiral structure. The unpolarized neutron measurements of superlattices on MgO were not able to determine if the commensurate structure they observed was from non-collinear Cr order. At thicknesses above 45 ML where long-period coupling is no longer observed, and at low temperatures where Cr is in an ISDW state, the Fe films are not magnetically coupled. In this thickness region, Schreyer et al. [83] found a transition to commensurate order with increasing temperature while Fullerton et al. [76,78] found a transition to paramagnetic order. This is the major remaining discrepancy in the results; it can be attributed to differences in the interface structure of the sputtered and MBE-grown samples.

10. Fe/Cr superlattices: interpretation

The coupling in superlattices is strongly influenced by the presence of a high degree of disorder and the resulting spin frustration. There are many possible states for Cr in these disordered superlattices. Fullerton et al. [76,78,79] interpret their results in terms of a transition between a high-temperature paramagnetic state in which there is no antiferromagnetic order and a low-temperature ISDW state with the nodes near the interfaces. In the ISDW state, the frustration is believed to be taken up by interface domain walls discussed in connection with Fig. 3c. These walls connect the Fe steps as illustrated schematically by the thick lines in Fig. 20. While nearly perfect interfaces appear to favor antinodes at the interfaces, it is plausible that disordered interfaces favor nodes close to the interface because then the moments are reduced where there is frustration in the coupling with the Fe. The domain walls parallel to the interface in the Cr essentially decouple Cr antiferromagnetic order from the Fe ferromagnetic order, as illustrated by the dotted line in Fig. 20. The resulting coupling between Fe layers is small, presumably because none of the Fe layers are coupled to the Cr.

Bulk Cr makes a transition into the paramagnetic state as the temperature is increased above the Néel temperature. The resistance anomaly found

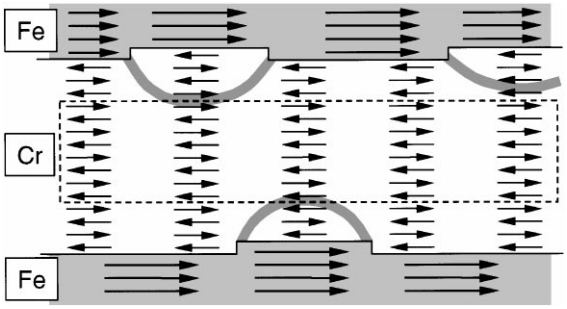

Fig. 20. A representation of the possible relief of spin frustration in antiferromagnetic Cr spacers in superlattices leading to the ISDW state. The heavy lines schematically indicate domain walls terminated at interfacial steps. The spin frustration is relieved by these walls near the interface leaving a region, shown by the dashed line, of ISDW ordered Cr [79].

by Fullerton et al. [76] is consistent with this type of transition. As the thickness decreases, the Néel temperature also decreases, either due to the decoupled antiferromagnetic state behaving like a thin film, or due to the increasing spin frustration due to the closer interfaces. Below a certain thickness, it is no longer favorable to fit in a half period of the ISDW, and the Cr goes into a different state [78]. There are indications of weak commensurate antiferromagnetic order for these thin Cr layers. The Cr may be paramagnetic in parts of the sample and commensurate in others, or may be in a strongly disordered commensurate state. Fishman [89] has derived a phase diagram consistent with this by considering a model in which the Cr moment is constrained to be zero at both interfaces. With this rigid constraint, he predicts an oscillatory component to the transition temperature. These oscillations have not been seen. Relaxing the strict constraint of the moments being zero exactly at the interface may weaken these oscillations [89]. Above the transition temperature, Fullerton et al. [74] observe a combination of long-period coupling and biquadratic coupling which can be interpreted in terms of a thickness fluctuation mechanism [31].

As an alternate to taking up the frustration in domain walls parallel to the interface, the frustration could be taken up in domain walls perpendicular to the interface, allowing the Cr moments to twist, as shown in Fig. 21. The resulting helical state is yet another possible state for the Cr that is found theoretically to be favorable in some situations [24,25,90]. In this case, regions of thickness that differ by one layer of Cr favor coupling in opposite directions. In these regions, the twist has different senses of rotation leading to a non-collinear coupling of subsequent Fe layers as described by Slonczewski's torsion or proximity magnetism model [23]. Whether domain walls parallel or perpendicular to the interfaces are favored depends on many different properties of the samples including the temperature and the average step spacing.

Schreyer et al. [83] interpret their results in terms of the incommensurate state described above at large thicknesses and low temperature and the paramagnetic state at high temperatures, both consistent with the results of Fullerton et al. [76,78]. However, they observe a commensurate, helical Cr state in a temperature range between the incommensurate state and the paramagnetic state. In a certain range, they find a coexistence of incommensurate order and commensurate order, presumably in different parts of the sample. It may be that the terrace lengths in these samples of Schreyer et al. [83] are larger than those in the samples of Fullerton et al. [76,78], allowing the commensurate, helical state to develop for certain samples and temperatures. In the samples of Fullerton et al., smaller terrace lengths could cause frustration at the interface sufficient to keep the Fe from inducing

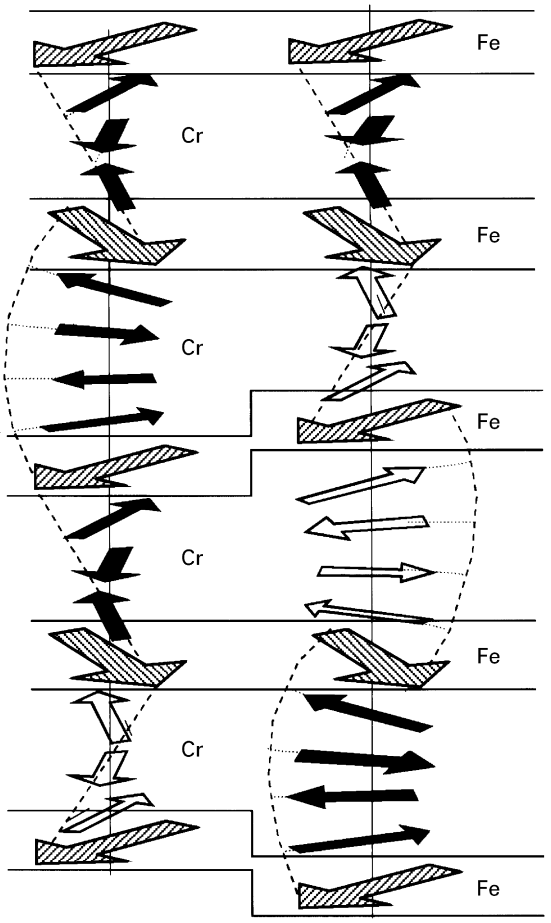

Fig. 21. Schematic illustration of non-collinearly coupled Fe layers showing how the energy is minimized in the presence of a Cr thickness fluctuation by a spiral rotation of the Cr moments. The empty and filled small arrows indicate an opposing sense of rotation of the Cr moments [83].

antiferromagnetic order in the Cr. Alternatively, there could be CSDW order in domains, but if the structure causes the domains to be sufficiently small, they are averaged over by the neutrons, and the CSDW order would not be observed [91]. In either case a resistivity anomaly is expected [13,14,92].

Schreyer et al. [83] support the description of their results in terms of the torsion model by noting that in magnetic hysteresis measurements by MOKE they observe the gradual approach to saturation predicted by Slonczewski's torsion model [23]. However, the gradual approach to saturation is only observed on the superlattices, not on trilayers prepared the same way on either GaAs or Al_2O_3 substrates [86]. Two explanations for this difference between the superlattices and the trilayers are the following. If there were variations in $\bar{J}_1$ or $\bar{J}_2$ due to variations in thickness of one spacer layer to the next, or if there were lateral variations in $\bar{J}_1$ or $\bar{J}_2$ within the MOKE laser spot size, both of which might not be unexpected for a superlattice, such variations would have the effect of rounding the hysteresis curves as previously described [36]. Alternatively, the interface structure of the superlattices may be sufficiently different from the trilayers requiring a different description of the coupling that includes aspects of the torsion model.

11. Conclusions

Interlayer exchange coupling through a Cr spacer layer is special because the Cr can be in various states of magnetic order itself. The coupling depends intimately on the ordering in the Cr, whether it has ISDW order, CSDW order, or is paramagnetic. The roughness distribution at the interface, both vertically and laterally, also strongly affects the magnetic coupling. In particular, the interface roughness frustrates the preferred alignments of the magnetic moments in the multilayer. Even when the system has found its lowest energy configuration, some pairs of moments are frustrated. Using what is known about the multilayer, particularly about the interface structure, measurements of the magnetic configuration can be interpreted in terms of models that describe different ways of minimizing the frustration.

The magnetic coupling in Fe/Cr/Fe(0 0 1) trilayers grown on Fe whiskers, where the growth is optimized to approach ideal layer-by-layer growth, is best understood. In this case, the interface morphology is relatively simple and for the most part can be taken into account. There is strong evidence in the temperature dependence of the phase slip that the short-period bilinear coupling is tied to the SDW state of the Cr spacer. The experimental results are consistent with CSDW order up to a Cr thickness where the first phase slip occurs and ISDW order beyond that. The short-period oscillatory coupling dominates the long-period coupling. The biquadratic coupling observed when the averaged short-period coupling goes to zero can be described by the Slonczewski thickness fluctuation model, which ignores possible antiferromagnetic order in the Cr [31]. However, there is no direct measurement of the Cr moments in these trilayers. Since the Cr is likely in an ordered state, its moments are likely to have a more complicated behavior than is implied by the conventional bilinear/biquadratic model of the coupling. Particularly when the Fe moments are not collinear, the Cr moments are also likely to be non-collinear. Thus, a complete description of the behavior of these samples will require treatment of non-collinear Cr moments [23–25,90]. On the other hand, the simple torsion model used to explain other measurements does not describe incommensurate order and hence cannot explain the existence of phase slips in the coupling or the behavior of the biquadratic coupling in these samples.

When the roughness at the interfaces increases due to different growth conditions or substrate conditions, the coupling changes dramatically. For room temperature growth, which produces roughness with a short terrace lengths, long-period oscillatory bilinear coupling dominates. The long-period coupling is consistent with the conventional model for coupling and is associated with a part of the Cr Fermi surface that is largely insensitive to the presence or absence of antiferromagnetic order in the Cr. Over the lateral response length l of the Fe layer, thickness fluctuations greatly reduce the

contribution of the short-period oscillatory coupling. The biquadratic coupling, which can be observed for Fe whisker samples near zeros in the long-period coupling, varies with the strength of the unaveraged short-period oscillations J_S, suggesting these still exist even if they are obscured by the thickness fluctuations. For moderate roughness with longer terrace lengths, different coupling is observed for the interfaces of Fe/Cr/Fe grown on Fe whiskers or on GaAs. For the trilayer on the Fe whisker, the long-period bilinear coupling dominates, but it is modulated by a short-period non-collinear component. For the trilayer on GaAs, the biquadratic coupling dominates, but long-period oscillations of the bilinear coupling are still observed.

In the case of superlattices, much of the experimental effort has been aimed at determining the state of the Cr magnetic order in coupled multilayers. Although there are still some discrepancies in the experimental results, presumably related to the interface structure, measurements of superlattices grown in very different ways on different substrates do show significant similarities that allow a coherent picture to be developed for these samples. The interfaces in the superlattices are rougher than the trilayers. As for the trilayers, the growth temperature of superlattices strongly affects the structure and magnetic properties. In the superlattices, there are regions of Cr thickness and temperature where the Cr is essentially uncoupled from the Fe layers; in this case, bulk-like ISDW properties are observed. In other regions of temperature and Cr thickness, novel spiral spin structures were observed and the magnetic coupling was stronger.

As one of the very few lattice-matched transition-metal pairs with one of the materials ferromagnetic, Fe/Cr multilayers offer excellent opportunities for investigating the exchange coupling of ferromagnetic layers through an antiferromagnetic spacer layer. The presence of antiferromagnetism in the Cr, and several different types at that, makes it a very rich system to study. Consistent explanations of the many seemingly disparate magnetic coupling measurements lie in understanding how roughness influences spin frustration and the Cr magnetic order.

Acknowledgements

We wish to acknowledge very helpful communications with D.E. Bürgler, A. Davies, R.S. Fishman, E.E. Fullerton, P. Grünberg, B. Heinrich, J. Meersschaut, A. Schreyer, and J.A. Stroscio, including providing us with several results prior to publication. This work was supported in part by the Office of Naval Research.

References

[1] P. Grünberg, R. Schreiber, Y. Pang, M.B. Brodsky, H. Sowers, Phys. Rev. Lett. 57 (1986) 2442.
[2] M.N. Baibich, J.M. Broto, A. Fert, F. Nguyen Van Dau, F. Petroff, P. Etienne, G. Creuzet, A. Friederich, J. Chazelas, Phys. Rev. Lett. 61 (1988) 2472.
[3] G. Binasch, P. Grünberg, F. Saurenbach, W. Zinn, Phys. Rev. B 39 (1989) 4828.
[4] S.S.P. Parkin, N. More, K.P. Roche, Phys. Rev. Lett. 64 (1990) 2304.
[5] J. Unguris, R.J. Celotta, D.T. Pierce, Phys. Rev. Lett. 67 (1991) 140.
[6] S.T. Purcell, W. Folkerts, M.T. Johnson, N.W.E. McGee, K. Jager, J. aan de Stegge, W.B. Zeper, W. Hoving, P. Grünberg, Phys. Rev. Lett. 67 (1991) 903.
[7] D.M. Edwards, J. Mathon, R.B. Muniz, M.S. Phan, Phys. Rev. Lett. 67 (1991) 493.
[8] P. Bruno, J. Magn. Magn. Mater. 121 (1993) 248.
[9] M.D. Stiles, Phys. Rev. B 48 (1993) 7238.
[10] P. Bruno, Phys. Rev. B 52 (1995) 411.
[11] M.D. Stiles, J. Magn. Magn. Mater. 200, this issue.
[12] J. Unguris, R.J. Celotta, D.T. Pierce, Phys. Rev. Lett. 79 (1997) 2734.
[13] E. Fawcett, Rev. Mod. Phys. 60 (1988) 209.
[14] E. Fawcett, H.L. Alberts, V.Y. Galkin, D.R. Noakes, J.V. Yakhmi, Rev. Mod. Phys. 66 (1994) 25.
[15] Z.P. Shi, R.S. Fishman, Phys. Rev. Lett. 78 (1997) 1351.
[16] A. Vega, D. Stoeffler, H. Dreyssé, C. Demangeat, Europhys. Lett. 31 (1995) 561.
[17] D. Stoeffler, F. Gautier, J. Magn. Magn. Mater. 147 (1995) 260.
[18] A. Berger, H. Hopster, Phys. Rev. Lett. 73 (1994) 193.
[19] A. Berger, E.E. Fullerton, J. Magn. Magn. Mater. 165 (1997) 471.
[20] R. Ribas, B. Dieny, Phys. Lett. A 167 (1992) 103.
[21] M. Rührig, A. Hubert, J. Magn. Magn. Mater. 121 (1993) 330.
[22] D. Stoeffler, F. Gautier, Phys. Rev. B 44 (1991) 10389.
[23] J.C. Slonczewski, J. Magn. Magn. Mater. 150 (1995) 13.
[24] M. Freyss, D. Stoeffler, H. Dreyssé, Phys. Rev. B 54 (1996) 12667.
[25] M. Freyss, D. Stoeffler, H. Dreyssé, J. Appl. Phys. 81 (1997) 4363.

[26] M. Rührig, R. Schäfer, A. Hubert, R. Mosler, J.A. Wolf, S. Demokritov, P. Grünberg, Phys. Stat. Sol. (a) 125 (1991) 635.
[27] B. Heinrich, J.F. Cochran, M. Kowalewski, J. Kirschner, Z. Celinski, A.S. Arrott, K. Myrtle, Phys. Rev. B 44 (1991) 9348.
[28] U. Köbler, K. Wagner, R. Wiechers, A. Fuss, W. Zinn, J. Magn. Magn. Mater. 103 (1992) 236.
[29] J.F. Cochran, J. Magn. Magn. Mater. 147 (1995) 101.
[30] P. Bruno, C. Chappert, Phys. Rev. B 46 (1992) 261.
[31] J.C. Slonczewski, Phys. Rev. Lett. 67 (1991) 3172.
[32] S.O. Demokritov, J. Phys. D 31 (1998) 925.
[33] S.O. Demokritov, E. Tysmbal, P. Grünberg, W. Zinn, I.K. Schuller, Phys. Rev. B 49 (1994) 720.
[34] A.S. Arrott, B. Heinrich, S.T. Purcell, in: M.G. Lagally (Ed.), Kinetics of Ordering and Growth at Surfaces, Plenum, New York, 1990, p. 321.
[35] J.A. Stroscio, D.T. Pierce, J. Vac. Sci. Technol. B 12 (1994) 1783.
[36] B. Heinrich, J.F. Cochran, T. Monchesky, R. Urban, Phys. Rev. 59 (1999) 14520.
[37] J.A. Stroscio, D.T. Pierce, J. Unguris, R.J. Celotta, J. Vac. Sci. Technol. B 12 (1994) 1789.
[38] A. Davies, J.A. Stroscio, D.T. Pierce, R.J. Celotta, Phys. Rev. Lett. 76 (1996) 4175.
[39] A. Davies, J.A. Stroscio, D.T. Pierce, J. Unguris, R.J. Celotta, J. Magn. Magn. Mater. 165 (1997) 82.
[40] J.A. Stroscio, D.T. Pierce, A. Davies, R.J. Celotta, M. Weinert, Phys. Rev. Lett. 75 (1995) 2960.
[41] D. Venus, B. Heinrich, Phys. Rev. B 53 (1996) R1733.
[42] B. Heinrich, J.F. Cochran, D. Venus, K. Totland, C. Schneider, K. Myrtle, J. Magn. Magn. Mater. 156 (1996) 215.
[43] R. Pfandzelter, T. Igel, H. Winter, Phys. Rev. B 54 (1996) 4496.
[44] D.T. Pierce, R.J. Celotta, J. Unguris, J. Appl. Phys. 73 (1993) 6201.
[45] J. Unguris, R.J. Celotta, D.T. Pierce, Phys. Rev. Lett. 69 (1992) 1125.
[46] M.R. Scheinfein, J. Unguris, M.H. Kelley, D.T. Pierce, R.J. Celotta, Rev. Sci. Instrum. 61 (1990) 2501.
[47] D.T. Pierce, J. Unguris, R.J. Celotta, in: B. Heinrich, J.A.C. Bland (Eds.), Ultrathin Magnetic Structures II, Springer, Heidelberg, 1994, p. 117.
[48] D.T. Pierce, J.A. Stroscio, J. Unguris, R.J. Celotta, Phys. Rev. B 49 (1994) 14564.
[49] F.U. Hillebrecht, C. Roth, R. Jungblut, E. Kisker, A. Bringer, Europhys. Lett. 19 (1992) 711.
[50] P.D. Johnson, N.B. Brookes, Y. Chang, Mater. Res. Soc. Symp. Proc. 231 (1992) 49.
[51] M. Freyss, D. Stoeffler, H. Dreyssé, Phys. Rev. B 56 (1997) 6047.
[52] S.A. Werner, A. Arrott, H. Kendrick, Phys. Rev. 155 (1967) 528.
[53] J. Unguris, R.J. Celotta, D.A. Tulchinsky, D.T. Pierce, J. Magn. Magn. Mater., in press.
[54] B. Heinrich, J.F. Cochran, Adv. Phys. 42 (1993) 523.
[55] S. Mirbt, A.M.N. Niklasson, B. Johansson, H.L. Skriver, Phys. Rev. B 54 (1996) 6382.
[56] M. van Schilfgaarde, F. Herman, Phys. Rev. Lett. 71 (1993) 1923.
[57] S. Mirbt, B. Johansson, Phys. Rev. B 56 (1997) 287.
[58] R.W. Wang, D.L. Mills, Phys. Rev. B 46 (1992) 11681.
[59] Y. Wang, P.M. Levy, J.L. Fry, Phys. Rev. Lett. 65 (1990) 2732.
[60] Z.P. Shi, P.M. Levy, J.L. Fry, Phys. Rev. B 49 (1994) 15159.
[61] D. Stoeffler, F. Gautier, Prog. Theor. Phys. Suppl. 101 (1990) 139.
[62] Z.P. Shi, R.S. Fishman, Phys. Rev. Lett. 78 (1997) 1351.
[63] R.S. Fishman, Z.P. Shi, J. Phys.: Condens. Matter 10 (1998) L277.
[64] R.S. Fishman, Z.P. Shi, Phys. Rev. B 59 (1999) 13849.
[65] S. Demokritov, J.A. Wolf, P. Grünberg, Europhys. Lett. 15 (1991) 881.
[66] P. Grünberg, S. Demokritov, A. Fuss, R. Schreiber, J.A. Wolf, S.T. Purcell, J. Magn. Magn. Mater. 104–107 (1992) 1734.
[67] J.A. Wolf, Q. Leng, R. Schreiber, P. Grünberg, W. Zinn, J. Magn. Magn. Mater. 121 (1993) 253.
[68] P. Grünberg, J.A. Wolf, R. Schäfer, Physica B 221 (1996) 357.
[69] C.M. Schmidt, D.E. Bürgler, D.M. Schaller, F. Meisinger, H.J. Güntherodt, Phys. Rev. B 60 (5) (1999), in press.
[70] D.E. Bürgler, private communication.
[71] M.D. Stiles, Phys. Rev. B 54 (1996) 14679.
[72] L. Tsetseris, B. Lee, Y.C. Chang, Phys. Rev. B 55 (1997) 11586.
[73] L. Tsetseris, B. Lee, Y.C. Chang, Phys. Rev. B 56 (1997) R11392.
[74] E.E. Fullerton, M.J. Conover, J.E. Mattson, C.H. Sowers, S.D. Bader, Phys. Rev. B 48 (1993) 15755.
[75] S. Adenwalla, G.P. Felcher, E.E. Fullerton, S.D. Bader, Phys. Rev. B 53 (1996) 2474.
[76] E.E. Fullerton, K.T. Riggs, C.H. Sowers, S.D. Bader, Phys. Rev. Lett. 75 (1995) 330.
[77] E.E. Fullerton, J.E. Mattson, C.H. Sowers, S.D. Bader, Scr. Metall. Mater. 33 (1995) 1637.
[78] E.E. Fullerton, S.D. Bader, J.L. Robertson, Phys. Rev. Lett. 77 (1996) 1382.
[79] E.E. Fullerton, C.H. Sowers, S.D. Bader, Phys. Rev. B 56 (1997) 5468.
[80] A. Schreyer, J.F. Ankner, T. Zeidler, H. Zabel, C.F. Majkrzak, M. Schäfer, P. Grünberg, Europhys. Lett. 32 (1995) 595.
[81] A. Schreyer, J.F. Ankner, T. Zeidler, H. Zabel, M. Schäfer, J.A. Wolf, P. Grünberg, C.F. Majkrzak, Phys. Rev. B 52 (1995) 16066.
[82] K. Theis-Bröhl, I. Zoller, P. Bödeker, T. Schmitte, H. Zabel, L. Brendel, M. Belzer, D.E. Wolf, Phys. Rev. B 57 (1998) 4747.
[83] A. Schreyer, C.F. Majkrzak, T. Zeidler, T. Schmitte, P. Bödeker, K. Theis-Bröhl, A. Abromeit, J.A. Dura, T. Watanabe, Phys. Rev. Lett. 79 (1997) 4914.

[84] J.F. Ankner, H. Kaiser, A. Schreyer, T. Zeidler, H. Zabel, M. Schäfer, P. Grünberg, J. Appl. Phys. 81 (1997) 3765.
[85] A. Schreyer, J.F. Ankner, M. Schäfer, H. Zabel, C.F. Majkrzak, P. Grünberg, Physica B 221 (1996) 366.
[86] A. Schreyer, private communication.
[87] J. Meersschaut, J. Dekoster, R. Schad, P. Beliën, M. Rots, Phys. Rev. Lett. 75 (1995) 1638.
[88] J. Meersschaut, Dissertation, Katholieke Universiteit Leuven, 1998.
[89] R.S. Fishman, Phys. Rev. B 57 (1998) 10284.
[90] R.S. Fishman, Phys. Rev. Lett. 81 (1998) 4979.
[91] E.E. Fullerton, private communication.
[92] B.M. Geerken, R. Griessen, G. Benediktsson, H.U. Åström, C. van Dijk, J. Phys. F 12 (1982) 603.